The Delplot Kinetic Method Applied to Systems with Adsorbates: Hydrodeoxygenation of Benzofuran on a Bimetallic CoPd Phosphide Catalyst Supported on KUSY

William J. Movick[b,†], Gwang-Nam Yun[c,d,†], I. Tyrone Ghampson[b,e], S. Ted Oyama[a,b,c*]

[a]School of Chemical Engineering, Fuzhou University, Fuzhou 350116, China

[b]Department of Chemical Systems Engineering, The University of Tokyo, 7-3-1 Hongo, Bunkyo-ku, Tokyo 113-8656, Japan

[c]Department of Chemical Engineering, Virginia Tech, Blacksburg, VA 24061, United States

[d]Green Carbon Research Center, Korea Research Institute of Chemical Technology (KRICT), 141 Gajeong-ro, Yuseong-gu, Daejeon 34114, Republic of Korea.

[e]Department of Applied Chemistry for Environment, Graduate School of Urban Environmental Sciences, Tokyo Metropolitan University, 1-1 Minami-osawa, Hachioji, Tokyo 192-0397, Japan

† These authors contributed equally to the content of the paper.

* Corresponding author.E-mail address: oyama@vt.edu (S. Ted Oyama)

Abstract

The Delplot method provides a means of analyzing conversion and selectivity data to derive a reaction sequence and has been applied so far to gas-phase or liquid-phase species. This study analyses the applicability of the method for catalytic reactions and considers for the first time adsorbed intermediates. The method is applied to a contact time study of the hydrodeoxygenation (HDO) of benzofuran at 0.5 MPa and 350 °C over a catalyst consisting of bimetallic CoPd phosphide supported on a potassium ion-exchanged ultra-stable Y (KUSY) zeolite. Both simple and detailed reaction networks were derived. The simple network considered gas-phase species only and were modeled by a first-order sequence of steps, whereas the detailed network took into account adsorbed intermediates and was simulated using a rake mechanism. The networks were compared using F-statistics, which accounted for the differences in the number of fitting parameters. The detailed network gave a better fit to the experimental data because it represented a more realistic description of the transformation. A suggested sequence from the Delplot method was consistent with the simple network but not with the detailed network. The lack of applicability of the Delplot analysis to the network with adsorbates was linked to overly large equilibrium constants, a determination supported by Delplot fitting for a model sequence. This study indicated the inapplicability of the Delplot method in determining reaction sequences that involve adsorbed species with large equilibrium constants for formation.

Keywords: CoPd phosphide; hydrodeoxygenation; benzofuran; rake mechanism; reaction network; Delplot analysis

1. Introduction

The determination of the steps constituting a reaction network is an important aspect of the analysis of reaction sequences and, according to Boudart, must be studied as a whole [1], with the objective of determining rate constants [2]. Boudart states that obtaining the rate is the essential goal of catalytic research, as catalysis is essentially a kinetic phenomenon [3,4]. Textbooks cover only simple reaction sequence [5,6,7,8]. Generally, the sequence is obtained by measuring selectivity or yield as a function of time [1]: contact time or space velocity in flow reactors [9] and real time in batch reactors [10]. A substantial development in this area was the Delplot method developed by Bhore et al. [11,12]. This method involves the analysis of plots of yield curves versus conversion, where the product yields are divided by various powers of the conversion to produce different "ranks". Extrapolation of these yields to zero conversion is used to determine whether the products are primary, secondary, or higher order. The method was applied to a parallel-series network at isothermal conditions and has been adopted by several studies to derive reaction networks, including studies in methane partial oxidation [13], hydrogenation of acrolein [14], hydrogenolysis of glycerol [15], hydrodenitrogenation of propylamine [16], hydrodeoxygenation of anisole [17], hydrothermal reaction of acetaldehyde [18], and the reaction of tetraalanine [19]. In subsequent studies, Klein and collaborators extended the method to examine the effects of products formed in multiple pathways [20], temperature [21], reversibility [22], and reaction intermediates [23], giving general guidelines on its use. The method and its applicability will be considered in detail in the present work. The original method was based on fluid-phase species and so are the various extensions and the examples listed above. In this work the role of adsorbates will be analyzed for the first time.

Hydrodeoxygenation (HDO) is involved in the upgrading of bio-oils derived from biomass and also takes part in the refining of petroleum feedstocks. Bio-oils derived from the pyrolysis of lignocellulosic biomass can have up to 40 wt% oxygen [24] in the form of organic acids, aldehydes, ketones, furans, phenolic compounds, guaiacols, syringols and sugar based compounds [25], while crude oil can contain up to 2 wt.% oxygen [26] mostly in the form of aromatic compounds. The high content of oxygenated compounds in bio-oil results in a low heating value (16–19 MJ/kg) compared to that of fossil fuels which have higher heating value (40 to 45 MJ/kg) [27]. It is desirable for fuels derived from both biomass and fossil resources to have lower oxygen content to elevate the heating value and also reduce acidity and viscosity. This study deals with the HDO of the model compound benzofuran, which is present in both bio-oil and conventional crude oil.

Benzofuran is an oxygen-containing heterocycle consisting of fused benzene and furan rings. Previous studies have reported that the transformation of benzofuran on solid catalysts typically begins with an initial step of hydrogenation of the furan ring, followed by either ring-opening of the ether linkage or hydrogenation of the benzene ring [28]. Subsequent steps include hydrogenation and cleavage of C-O and C-C bonds. These steps have been reported on noble metals [29,30] and multi-component catalysts such as transition metal sulfides [31,32,33], nitrides [34] and phosphides [35]. The latter has advantage over noble metals in price, over sulfides in not requiring a sulfiding agent to sustain activity, and over nitrides in activity. Phosphides of base metals have been shown to be effective HDO catalysts for various compounds [36,37,38,39,40,41,42], and in many cases were found to be more active than noble metal catalysts. The drawback of these materials is their high synthesis temperature and for that reason some researchers have added small amounts of noble metals (Ru, Os, Ir, Rh, and Pt) to

lower the temperature [43,44,45,46]. The resultant noble-metal doped phosphide catalysts were found to be more active than the base metal phosphide catalyst in the HDO of dibenzofuran at 175-300 °C and 3 MPa [43], phenol at 180-220 °C and 2 MPa [45], and guaiacol at 300 °C and 3 MPa [46].

In the present work a contact time analysis for CoPd(9:1)P/KUSY is used to deduce simple reaction networks which account for all observed gaseous products and more comprehensive networks which considers adsorbed intermediates. First-order kinetic analysis is used to simulate the networks to estimate rate constants and adsorption and desorption constants. The Delplot method can be used to determine the order in which products are formed in a sequence [11,12] and the applicability of the method to sequences with adsorbed species is studied. The Delplot method is found to agree with the kinetic analyses on simple sequences involving only gas-phase species but disagree on the detailed networks involving surface species. A simulation of a model sequence is used to explain the results. It is not the objective of this study to derive the kinetics of the reaction, but rather to study the sequence of steps, in a manner resembling an analysis reported by Boudart and Djéga-Mariadassou [47,48].

2. Experimental

2.1 Catalyst preparation and characterization

The catalyst was prepared by simultaneous impregnation of cobalt and palladium precursors onto a potassium ion-exchanged USY zeolite (KUSY) followed by reduction, as described elsewhere [49]. Briefly, the preparation of the catalyst involved three stages. First, potassium ion-exchange of a commercial HUSY zeolite (Si/Al = 40, CBV780, Zeolyst International) support was performed with an aqueous solution (0.5 M) of potassium nitrate

(KNO_3, Wako, > 99.0%), with the solid subsequently filtered, washed with deionized water, dried at 110 °C overnight, and calcined at 650 °C for 4 h. The procedure was repeated two more times in order to remove a majority of the acid sites [50]. Second, a precursor solution of cobalt (II) hydroxide ($Co(OH)_2$, Wako, 56.0-64.0% Co basis), palladium (II) acetate ($Pd(OAc)_2$, Aldrich, > 98%) and phosphorus acid (H_3PO_3, Aldrich, > 99%) in deionized water was used to impregnate the KUSY, which was then dried at 70 °C overnight. The dried sample was pelletized and sieved to particles of 650-1180 μm diameter. Third, the resulting particles were reduced in flowing H_2 (1000 cm^3 min^{-1} $g_{catalyst}^{-1}$) at 550 °C for 2 h. The reduction temperature was determined by temperature-programmed reduction (TPR) in separate experiments [49]. After reduction, the sample was cooled to room temperature in flowing N_2 (100 cm^3 min^{-1}) and passivated for 1 h in flowing 0.5% O_2/He (100 cm^3 min^{-1}). The metal-to-phosphorus ratio was 1:2, the cobalt-to-palladium ratio was 9:1, and the metal loading was 1.16 mmol $g_{support}^{-1}$ (Co = 1.04 mmol $g_{support}^{-1}$ and Pd = 0.12 mmol $g_{support}^{-1}$), corresponding to a weight loading of 4.6 wt% Co, 0.9 wt% Pd, and 2.5 wt% P. The catalyst was denoted as CoPd(9:1)P/KUSY.

Carbon monoxide (CO) uptake, measured by a pulse injection method using a catalyst analyzer (TPD-1-AT, BEL Japan, Inc.), was used to provide an estimate of the amount of active sites on the catalyst [51]. The passivated catalyst (300 mg) was re-reduced in flowing H_2 (100 cm^3 min^{-1}) at 500 °C for 2 h and then cooled to 50 °C in flowing He (100 cm^3 min^{-1}). Pulses of 3% CO/He were injected using a helium carrier (100 cm^3 min^{-1}) and passed over the sample at 50 °C, and the mass 28 (CO) signal was monitored with a mass spectrometer to measure the total dynamic gas uptake. The BET method based on nitrogen adsorption isotherms at 77 K measured with a volumetric apparatus (BELSORP mini II, BEL Japan, Inc.) was used to obtain the specific surface area of the catalyst. The passivated catalyst (60 mg) was evacuated and dried at 300 °C

for 4 h prior to the measurement. Transmission electron microscopy (TEM) images were used to estimate the average particle size of the catalyst. The passivated sample was ground to a fine powder, dispersed into ethanol using a sonicator, deposited on a carbon-coated copper grid, and dried at room temperature for 0.5 h in air. The images were obtained using an electron microscope (EM-002B, Topcon Corporation) operated at 120 kV. Extended X-ray absorption fine structure (EXAFS) spectra at the Co K-edge (7710 eV) of catalyst samples and a reference foil were recorded at beam line BL-12 C at the Photon Factory (PF) at the Institute of Materials Structure Science, High-Energy Accelerator Research Organization (KEK-IMSS-PF), Tsukuba, Japan. Measurements were taken in transmission mode under in situ conditions after re-reduction of the passivated sample at 500 °C for 2 h under a H_2 flow. The data were analyzed by the programs Athena and Artemis. Phase shift and amplitude functions were calculated by FEFF8.

2.2. Contact time (CT) analysis

The reactivity of the catalyst in HDO as a function of contact time was measured at 0.5 MPa and 350 °C in a tubular fixed-bed reactor of 2.0 cm OD using benzofuran as a model compound. The passivated catalyst was loaded in the central section of the reactor with quartz sand of the same particle size as the catalyst to give a uniform flow in the catalyst bed. The catalyst was pretreated at 500 °C for 2 h in H_2 (1000 $cm^3\ g_{catalyst}^{-1}\ min^{-1}$) in order to remove the passivation layer. The catalyst was then cooled to 350 °C and stabilized in H_2 flow (79 $cm^3\ min^{-1}$), and the total pressure was fixed at 0.5 MPa using a back-pressure regulator. A vaporized feed consisting of the reactant 98 wt% benzofuran (TCI, > 99.0%) and an internal standard 2 wt% decalin (TCI, > 98.0%) was delivered using a liquid pump to a vaporizer held at 250 °C. The feed was delivered along with a H_2 flow to achieve a feed concentration of 3 mol% benzofuran

in H_2. The concentration of benzofuran can be calculated to be C = (0.03)(0.5MPa)(10^6 Pa MPa^{-1})/(8.314 m^3Pa/mol K)(623 K)(10^6 cm^3m^{-3}) = 2.9 x 10^{-6} mol/cm^3. The decalin did not react at the reaction conditions used in this study. The rate of reaction is expressed as a turnover frequency (TOF) based on sites titrated by the chemisorption of CO. The TOF is obtained at differential conditions, where conversion is linear with contact time.

$$TOF\ (s^{-1}) = \frac{Benzofuran\ flow\ rate\ (\mu mol\ s^{-1})X}{Catalyst\ weight\ (g)x\ CO\ uptake\ (\mu mol\ g^{-1})} \quad (1)$$

After introducing the feed, the catalyst was allowed to reach steady state for 12 h. The reactant flow rate (3.4-10 μmol s^{-1}) and catalyst weight (0.03-0.1 g) were varied in order to achieve different contact times (τ), which are defined based on the number of sites:

$$Contact\ time\ (s) = \tau = \frac{Catalyst\ weight\ (g)\times CO\ uptake\ (\mu mol/g)}{Benzofuran\ flowrate\ (\mu mol/s)} \quad (2)$$

Contact times (CTs) may be defined on the basis of volume, weight, or as here, the number of sites. The basis of volume is most familiar and is used principally in reactor studies where it is called a space time or a residence time [52]. The basis of weight is commonly used in hydroprocessing applications [53]. The basis of sites is used in catalytic studies where the number of sites can be estimated and has been called the site time [54]. There are significant advantages for using a contact time based on sites for kinetic studies as summarized in Table 1.

Table 1. Advantages of Using Contact Times (τ) Based on Sites

τ is inversely related to the turnover frequency	Gives information about the rate
τ = 1 s corresponds to one turnover	Gives information on the usage of sites
The slope of conversion vs. τ is the TOF	Linearity indicates differential regime

First, from the definitions in Eqns (1) and (2), τ is given by the conversion (X) divided by the turnover frequency (TOF) as shown in Eqn (3). Thus, the basis of sites gives a measure of the rate, so that if a high τ is needed to achieve a given conversion, a low TOF is indicated.

$$\tau = \frac{X}{TOF} \tag{3}$$

Second, since the inverse TOF is also equal to the number of turnovers, τ = 1 s corresponds to one turnover (all sites have been used once). This is an ideal upper value to strive for since the activity of each site is then considered. Third, in plots of conversion versus site time, which will be displayed later, the slope is the TOF. This can be deduced from differentiation of Eqn (3). From these considerations, the basis of sites is the most appropriate for kinetic studies, of course with the proviso that the number of sites can be estimated. This can be difficult, for example for acid or base-catalyzed reactions where there is a distribution of sites, and in that case either an approximate order-of-magnitude estimate can be used or reversion can be made to a volumetric contact time.

The benzofuran flow rate and the H_2 flow rate were both adjusted to keep the feed concentration constant (3 mol% benzofuran in H_2), and the catalyst weight was adjusted along with the quartz sand amount to keep the bed volume constant (1.5 cm^3). The contact time was varied in the range of 0.04-0.70 s, and the measurements were started at the highest contact time and the times were varied downward and then upward to verify that a smooth trace was obtained, which is evidence that the catalyst was stable during the measurements. Reaction products were analyzed by an on-line gas chromatograph (Shimadzu GC-14A, DB-624) equipped with a flame ionization detector (FID). The carbon balance was calculated to be better

than 100 ± 1%. The conversion of benzofuran and selectivity to products were calculated by the following equations:

$$Conversion(\%) = \frac{\sum All\ products}{Moles\ of\ Benzofuran\ in\ feed} \times 100\% \quad (4)$$

$$Selectivity(\%) = \left(\frac{Moles\ of\ product}{Moles\ of\ total\ products}\right) \times 100\% \quad (5)$$

The total conversion was kept below 20%.

Proposed reaction networks were simulated by assuming that the reactions were first order. A set of ordinary differential equations (ODE) based on the disappearance rate of benzofuran (A) and the formation rate of products (P_i) was used to describe the networks, following a general form:

$$\frac{d[A]}{d\tau}\ or\ \frac{d[P_i]}{d\tau} = f(k_i, [A], [P_i]) \quad (6)$$

where k_i is the rate constant for each reaction step and [A] and [P_i] are the gas phase concentrations of benzofuran and the products in the effluent. A set of ODEs based on adsorbed benzofuran (A^*) and surface species (P^*) was also derived in the same manner:

$$\frac{d[A^*]}{d\tau}\ or\ \frac{d[P_i{}^*]}{d\tau} = g(k_i, [A], [P_i], [*], [A^*], [P_i{}^*]) \quad (7)$$

Here, [A^*] and [$P_i{}^*$] are the surface concentrations of adsorbates and [*] is the concentration of the vacant sites. The ODEs were solved by using a fitting software developed for this reaction system using GNU Octave [55]. First, random values for each reaction constant were chosen. Each constant was then independently adjusted to find the value that minimized the residual sum of squares (RSS) of the model, obtained through the equation:

$$RSS = \sum\left(y_{exp} - y_{pred}\right)^2 \quad (8)$$

In this equation, y_{exp} is the experimental mole fraction of each component and y_{pred} is the model prediction for this value. This procedure was looped, randomly choosing the order in which the parameters were minimized. For the first 60% of the minimization, occasional "bumps" were used by multiplying each constant by a random value. This was used in order to reduce the risk of falling into local minimum of the RSS. For the last 40% of the minimization, no "bumps" were used. The overall goodness of fit of each model was calculated by the R-squared value:

$$R^2 = 1 - \frac{\Sigma(y_{exp} - y_{pred})^2}{\Sigma(y_{exp} - y_{ave})^2} \quad (9)$$

In this equation, y_{ave} is the average mole fraction (different values were given to each of the reaction species). Multiple models were used and the goodness-of-fit for each was calculated. The statistical significance of increasing the number of reaction coefficients was determined through the F-test. For each case, the critical F-factor value was chosen for a false-rejection probability of 0.05. The F-statistic was calculated by the equation:

$$F = \frac{\left(\frac{RSS_1 - RSS_2}{p_2 - p_1}\right)}{\left(\frac{RSS_2}{n - p_2}\right)} \quad (10)$$

Here RSS_i is the residual sum of squares of model i, p_i is the number of parameters for model i, and n is the total number of data points.

3. Results and discussion

3.1. Characterization of CoPd(9:1)P/KUSY catalyst

The XRD pattern of the CoPd(9:1)P/KUSY sample is compared to those of CoP/KUSY, Pd_6P/KUSY, and the KUSY support (Fig. S1 in the Supplementary Information, SI). For the CoP sample there are small signals that are aligned with the location of the most intense features of the CoP reference (Powder diffraction file 29-0497), indicating the presence of CoP. For the

CoPd(9:1)P/KUSY sample only the lines of the KUSY support are visible (Fig. S1), indicating that the CoPd phase is highly dispersed.

Fig. 1 shows the EXAFS Fourier transforms of the Co K-edge of the CoPd(9:1)P/KUSY and CoP/KUSY samples and a reference Co foil. The measurements were carried out at in situ conditions on samples reduced at the same temperature (500 ^{o}C) as for reaction. The Co foil was fit using a one shell model based on the Co hcp crystal structure and an R range of 0.15-0.27 nm. The CoP was fit by a two-shell model that considered Co-Co and Co-P first order interactions over an R range of 0.10-0.30 nm. The CoP shows two main peaks corresponding to the Co-P bonding at 0.220 nm and Co-Co bonding at 0.260 nm. These are similar to the reference values of 0.227 nm for Co-P interactions and 0.267 nm for Co-Co interactions in CoP [56]. For bimetallic samples, a three-shell model was used, with one shell related to each Co-P, Co-Co, and Co-Pd bond interactions. The R range was also fixed at 0.10-0.30 nm. The bimetallic sample had a similar shape as the CoP material but with a slight decrease in the Co-Co bonding amplitude because of the presence of Pd, although a Co-Pd distance was not observed (expected at 0.263 nm [57]). This was probably because of the low amount of Pd. The Co-P bond distance was relatively unaffected by the addition of palladium. However, Co-Co bond distances shrank, to a value of 0.256 nm in CoPd(9:1)P/KUSY (as measured by EXAFS). This indicated an electronic effect of the Pd as confirmed for a series of CoPdP samples [49].

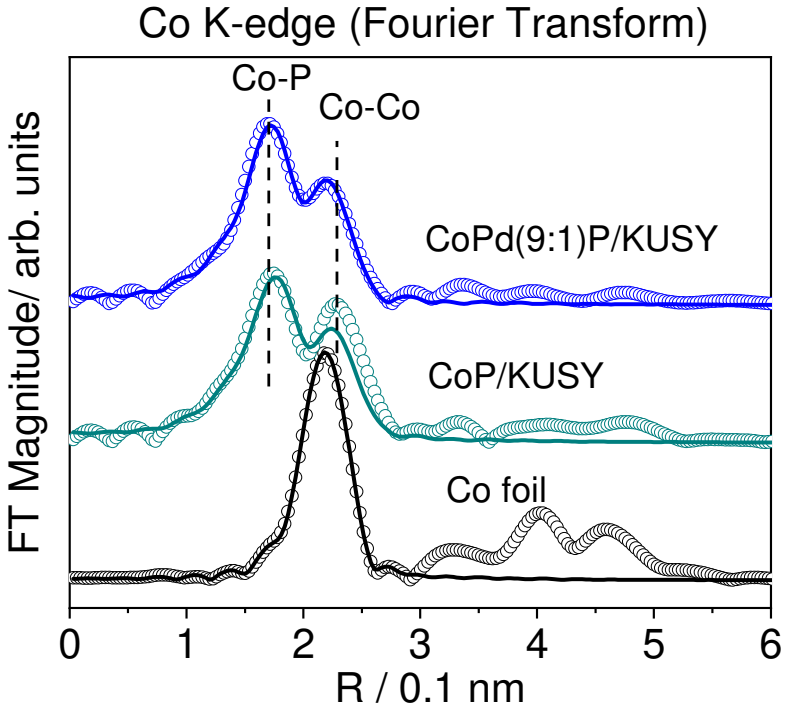

Figure 1. Magnitude of the Fourier transform of the Co K-edge EXAFS of samples re-reduced at 500 °C for 2 h in H_2 flow. Experimental data (open circles) and model fits (lines) are shown for each sample.

Table 2 shows the BET surface area (524 m^2 g^{-1}) and CO chemisorption (38 µmol g^{-1}) characterization results, and Fig. S2 shows a transmission electron microscopy (TEM) image with size distribution of 2-10 nm.

Table 2. Surface properties of CoPd(9:1)P/KUSY

Catalyst	BET area	CO uptake
CoPd(9:1)P/KUSY	524 m^2 g^{-1}	38 µmol g^{-1}

3.2. Determination of reaction networks

The present study investigates the steps in the hydrodeoxygenation of benzofuran using selectivity versus contact time measurements, and the results will be shown presently. A simple reaction network is proposed (Fig. 2) based on the measurements, which is largely in agreement with literature reports on the HDO of benzofuran and 2-ethylphenol [33,35,58,59,60].

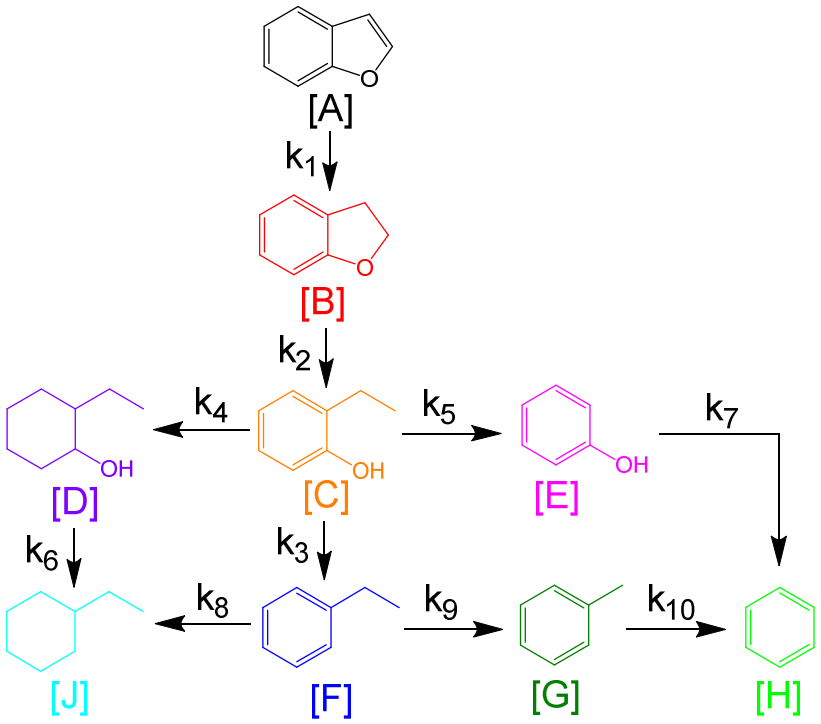

Figure 2. Base case reaction network (M1)

The network begins with the hydrogenation of the furan ring of benzofuran (A) to form 2,3-dihydrobenzofuran (B), followed by ring-opening to produce 2-ethylphenol (C). The reaction then splits into three different pathways. The first is hydrogenation of the benzene ring to form 2-ethylcyclohexanol (D) and its subsequent dehydroxylation to produce ethylcyclohexane. The second is hydrocracking of the ethyl group to form phenol (E) followed by deoxygenation to produce benzene. The third is deoxygenation to form ethylbenzene (F) which can then undergo

hydrocracking to form toluene (G) and subsequently benzene (H) or, alternatively hydrogenation to produce ethylcyclohexane (J). Based on prior work it is suggested that the Co sites, which were found to be intrinsically more active than the Pd sites, were likely involved in the initial steps and both Co and Pd sites were involved in later steps in the sequence [49].

The base case reaction network model M1 (Fig. 2) derived from the experimental data was used as the basis for eight models, four of which involved only gas-phase species (models M1-M4) and four dealt with both gas-phase and surface species (surface models SM1-SM4). The models were all based on first-order rate constants and differed only in the inclusion of reversible steps for the hydrogenation reactions (none for M1 and SM1, step 1 for M2 and SM2, steps 1, 4, 8 for M3 and SM3, steps 1, 2, 4, 8 for M4 and SM4). The models are presented in their entirety in the Supplementary Information (SI) section. Models M2 and SM2 will be discussed in the main body because they have low regression coefficients. A summary of the statistical results for the whole set is presented below (Table 3).

Table 3. Statistics on models used for fitting contact time data

	Gas-phase Mechanism				Adsorbate Mechanism				
# Reversible reactions	0	1	3	4	0	1	3	4	
	M1	M2	M3	M4	SM1	SM2	SM3	SM4	
R^2	0.747	0.809	0.783	0.847	0.822	0.874	0.858	0.867	
RSS	0.426	0.322	0.365	0.257	0.300	0.213	0.239	0.225	
p	10	11	13	14	27	28	30	31	
F-factor		M2 vs M1	M3 vs M1	M4 vs M1	SM1 vs M1	SM2 vs SM1	SM3 vs SM1	SM4 vs SM1	SM2 vs M2
Calculated		45.8	6.92	22.64	7.76	50.97	10.49	10.18	3.74
Critical (0.05)		3.91	1.69	2.44	2.67	3.92	2.68	2.45	1.71

The reported values include the regression coefficients, which give a measure of the goodness-of-fits, the number of parameters in the models (p), and the F-factor for a false-rejection probability of 0.05, used in the comparison of models with different number of parameters. A total of n=152 experimental points were used in all the models.

3.3. Contact time analysis and simple reaction network

Results for the simple gas-phase models M1-M4 are found in the SI section. Results for Model M2, which has one reversible step, are presented here. Selectivity results as a function of contact time at low conversion (< 20%) were used to determine the reaction network (Fig. 3). The top-left panel (Fig. 3a) shows the conversion of benzofuran and the selectivity to the main products (2-ethylphenol and 2, 3-dihydrobenzofuran), the top-right panel (Fig. 3b) shows the selectivity to products with low carbon number (toluene, phenol, and benzene), the bottom-left panel (Fig. 3c) shows the selectivity to products with high carbon number (ethylbenzene, 2-ethylcyclohexanol, and ethylcyclohexane), and the bottom-right panel (Fig. 3d) displays the network. Note should be made of the differences in scale for the selectivities. For selectivities below 2% there is considerable scatter in the points because of the low concentrations of products.

Model M2 differs from Model M1(details in SI) of Fig. 2 in one significant step, namely, a reversible transformation of 2,3-dihydrobenzofuran to 2-ethylphenol. Fig. 3 shows that the selectivities to these two main products level-out at high contact times (above 0.3 s), which could be due to an equilibrium step between them. This observation agrees with previously reported schemes [33,61].

The conversion increased linearly with contact time and did not exceed 20% (Fig. 3a). The slope gives the TOF, which can be calculated to be 0.28 s^{-1}. Since the plot is linear the results also indicate that the data are in the differential regime and suitable for a kinetic analysis. The Weisz-Prater criterion (C_{WP}) and the Thiele modulus (ϕ) were used to verify the absence of internal diffusion limitations (see SI). The highest value of C_{WP} was 7.1×10^{-4} and effectiveness factors from the Thiele modulus were close to unity, both of which satisfy the criteria for negligible diffusion limitations at the conditions employed in this work.

The selectivity to 2,3-dihydrobenzofuran decreased with increasing contact time as expected for a primary product. The selectivity to 2-ethylphenol increased initially and then leveled off at higher contact times, indicating that it is an intermediate product. The selectivities to phenol, ethylbenzene, and toluene showed considerable noise because of the low levels of these compounds, but all tended to start low, increase, and then level off (Fig. 3b and Fig. 3c), which are characteristics of intermediate products. The compounds benzene and ethylcyclohexane appeared only at higher contact times as expected for final products in a reaction network. It is acknowledged that there is significant error in each individual selectivity, but the various models used to describe the overall data were subject to statistical analysis (Table 3) and reasonable conclusions could be derived.

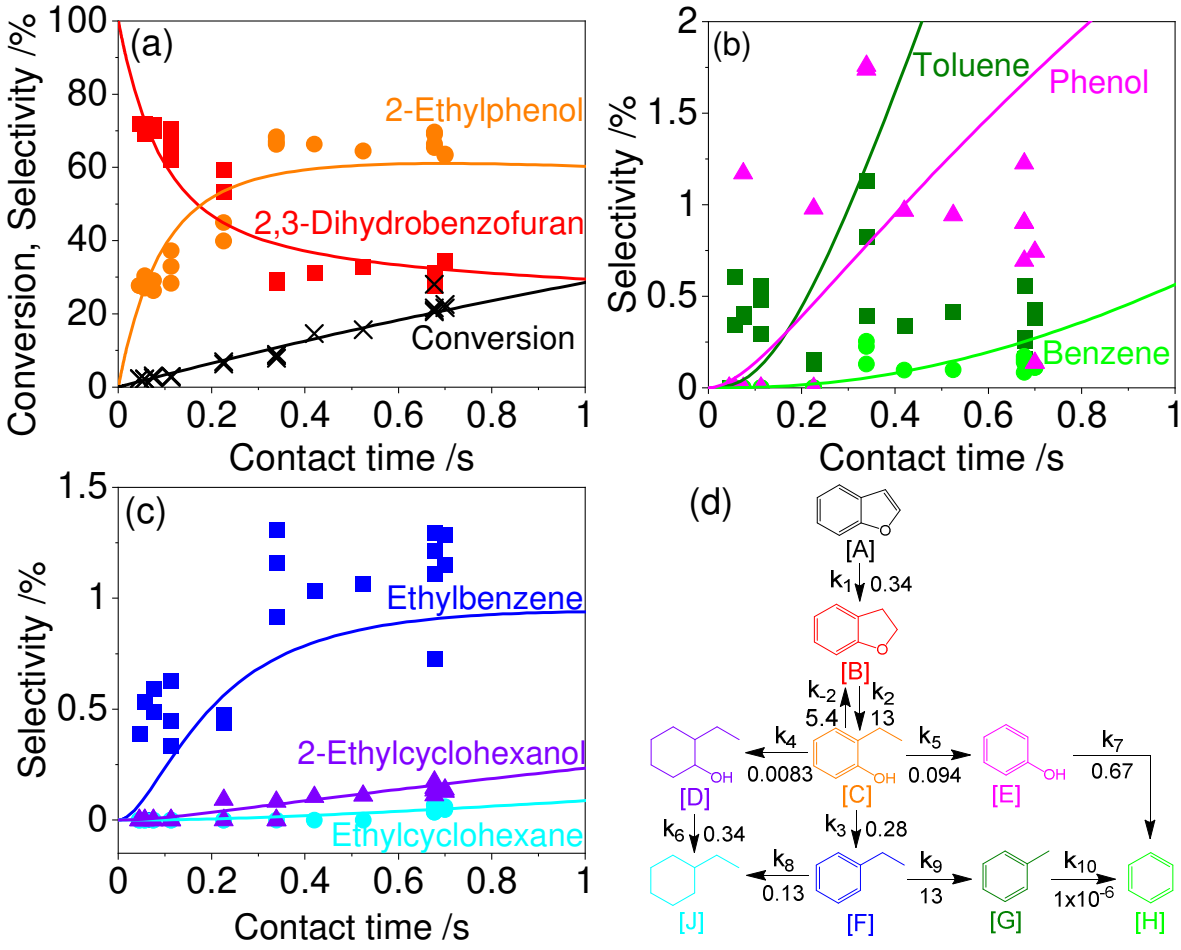

Figure 3. Model M2 experimental results (points). Contact time measurement of HDO of benzofuran at 0.5 MPa and 350 °C and calculated fits using M2 (continuous lines). (a) Conversion of benzofuran and product selectivity for 2,3-dihydrobenzofuran and 2-ethylphenol. (b) Product selectivity for toluene, phenol, and benzene. (c) Product selectivity for ethylbenzene, 2-ethylcyclohexanol, and ethylcyclohexane. (d) Proposed alternative simple reaction network of HDO of benzofuran using M2. One reversible reaction is considered. Calculated reaction constants are shown by each corresponding reaction step and have units of s^{-1}.

Mathematical modeling of the reaction network was used to obtain fitting results of the products selectivities (continuous lines in Fig. 3) and to determine rate constants. Although for brevity, the experimental fits for M1 are in the SI section, the kinetic analysis method and results for M1 and M2 are described here. Table 4 shows the set of ODEs used for the modeling which considered the main observed gas-phase species. The conversion was low (< 20%) and the

concentration of H_2 was high (97%) and assumed to be constant under the reaction conditions and hence not to influence the reaction kinetics. For the equations, as indicated before, each compound was assigned the following letters: benzofuran [A], 2,3-dihydrobenzofuran [B], 2-ethylphenol [C], 2-ethylcyclohexanol [D], phenol [E], ethylbenzene [F], toluene [G], benzene [H], and ethylcyclohexane [J], and reaction constants (k_1-k_{10}) were defined for each step. A differential equation numerical solver was used to obtain the model fit, and a minimization program specifically developed for this work was used to obtain the reaction constants, as described in Section 2.2.

Table 4. Rate expressions for observed gas phase species for M1 and M2

$\frac{d[A]}{d\tau} = -k_1[A]$	$\frac{d[F]}{d\tau} = k_3[C] - (k_8 + k_9)[F]$
$\frac{d[B]}{d\tau} = k_1[A] - k_2[B] + \{k_{-2}[C]\}^a$	$\frac{d[G]}{d\tau} = k_9[F] - k_{10}[G]$
$\frac{d[C]}{d\tau} = k_2[B] - (k_3 + k_4 + k_5)[C] - \{k_{-2}[C]\}^a$	$\frac{d[H]}{d\tau} = k_7[E] + k_{10}[G]$
$\frac{d[D]}{d\tau} = k_4[C] - k_6[D]$	$\frac{d[J]}{d\tau} = k_6[D] + k_8[F]$
$\frac{d[E]}{d\tau} = k_5[C] - k_7[E]$	

[a] Values in brackets { } are only used in M2

The results of the analysis give the fitted rate constants and regression coefficients (Table 5). The calculated rate constants for M2 (Table 5 and Fig. 3d) were similar to those of M1.

Table 5. Reaction rate constants and regression coefficients for models M1 and M2

Rate constant (s^{-1})	M1	M2	Rate constant (s^{-1})	M1	M2
k_1	0.32	0.34	k_6	1.3	0.34
k_2	7.3	13	k_7	0.62	0.67
k_{-2}	-	5.4	k_8	0.0033	0.13
k_3	0.28	0.22	k_9	16	13
k_4	0.0094	0.0083	k_{10}	1×10^{-6}	1×10^{-6}
k_5	0.11	0.094	R^2	0.747	0.809

For M2 the forward reaction rate constant (k_2 = 13 s^{-1}) for the reversible step is higher than the reverse reaction (k_{-2} = 5.4 s^{-1}), and both are higher than those of most of the other steps, suggesting quasi-equilibrium. The R^2 value for M2 fits was 0.809, an improvement over the value for the M1 fit of 0.747. This indicates that the existence of a reversible step in the reaction sequence better describes the HDO of benzofuran on CoPd(9:1)P/KUSY, although the poor fits to the low selectivity products (Fig. 3) suggest that the reaction scheme is still inadequate. A possible reason for the inadequacy is that the reaction network was modeled without consideration of surface species and thus ignores essential steps in the sequence. A more detailed model to address this shortcoming is discussed in the next section.

3.3. Detailed reaction network

Results for the surface models SM1-SM4 are found in the SI section. Results for model SM2, which is analogous to model M2, are presented here. A comprehensive reaction sequence which takes into account adsorbed intermediates based on a "rake" mechanism is proposed (Fig. 4) to further improve the model fit with contact time analysis. Surface species are shown in blue and gas-phase species in black. A rake mechanism considers steps on the surface where each intermediate can adsorb and desorb [62,63]. The suggested sequence in surface model SM2 involves all observed gas-phase species and their corresponding adsorbates but does not consider possible spectator species. This would require the use of in situ spectroscopic techniques and is beyond the scope of the present study. It was found previously that inclusion of adsorbed species to simulation models improves kinetic analysis and provides a more realistic description of the sequence [64,65]. The reaction network has surface transformations shown in the

horizontal direction and adsorption and desorption steps indicated in the vertical direction (Fig. 4). Table 6 lists the rate expressions for gas phase species which uses the same compound labeling as in M1 and M2. The symbol [*] denotes the concentration of vacant sites. Both adsorption and desorption steps of each observable species are considered, except for ethylcyclohexane in which only desorption is allowed as adsorption likely occurs more slowly than the other compounds as it is saturated. The reaction network of adsorbed species follows the same sequence as M2, including the reversible reaction between 2,3-dihydrobenzofuran and 2-ethylphenol. The sequence begins with the adsorption of benzofuran via the oxygen atom, followed by hydrogenation of the C=C bond to form an adsorbed 2,3-dibenzofuran intermediate, and a reversible ring-opening reaction to form an adsorbed 2-ethylphenoxide species. As previously shown, the reaction proceeds along three pathways to form intermediates which either desorb or subsequently transform to other adsorbed species. Table 7 shows the rate expressions for the adsorbed species and the total concentration of adsorption sites (L) which is calculated by dividing the CO uptake (38 μmol g^{-1}) by the surface area of the catalyst (524 m^2 g^{-1}). In the table, the concentration of the adsorbed species were represented as follows: benzofuran* = [A*], 2,3-dihydrobenzofuran* = [B*], 2-ethylphenol* = [C*], 2-ethylcyclohexanol* = [D*], phenol* = [E*], ethylbenzene* = [F*], toluene* = [G*], benzene* = [H*], and ethylcyclohexane* = [J*]. This follows the same nomenclature scheme presented earlier for gas-phase species.

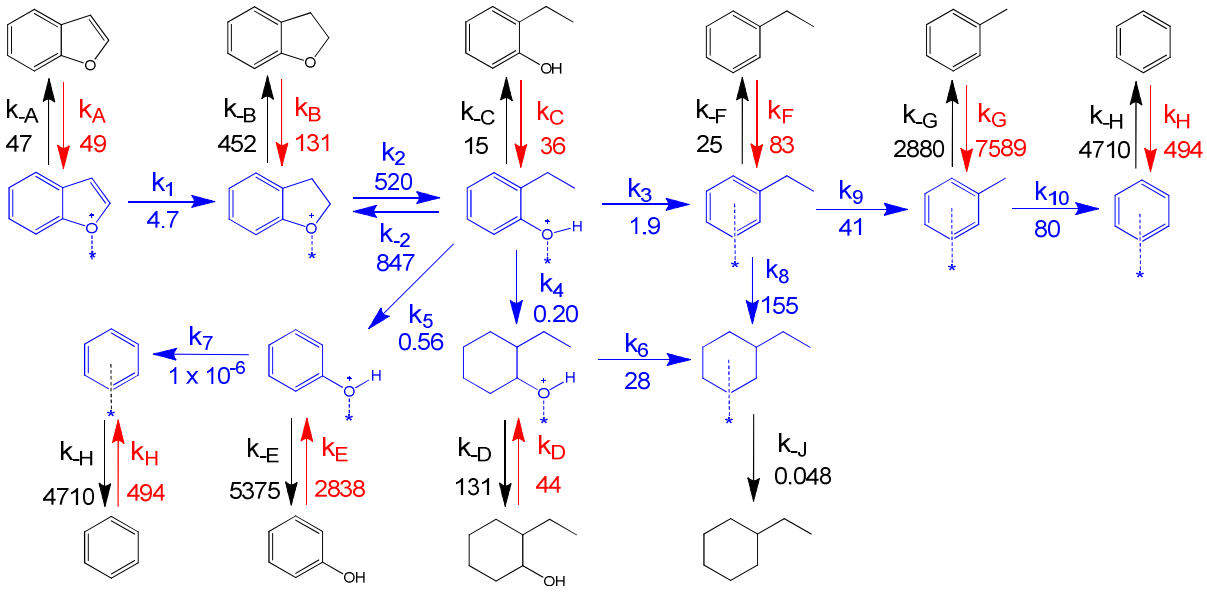

Figure 4. Proposed detailed reaction network of HDO of benzofuran using SM2. Adsorbed species and reaction rate constants are shown in blue, while adsorption rate constants are shown in red. Calculated reaction rate and desorption constants have units of s^{-1} and the adsorption rate constants have units of $cm^3\ \mu mol^{-1}\ s^{-1}$.

Table 6. Rate expressions for observable gaseous species in SM2

$\frac{V}{S}\frac{d[A]}{d\tau} = -k_A[A][*] + k_{-A}[A^*]$	$\frac{V}{S}\frac{d[F]}{d\tau} = -k_F[F][*] + k_{-F}[F^*]$
$\frac{V}{S}\frac{d[B]}{d\tau} = -k_B[B][*] + k_{-B}[B^*]$	$\frac{V}{S}\frac{d[G]}{d\tau} = -k_G[G][*] + k_{-G}[G^*]$
$\frac{V}{S}\frac{d[C]}{d\tau} = -k_C[C][*] + k_{-C}[C^*]$	$\frac{V}{S}\frac{d[H]}{d\tau} = -k_H[H][*] + k_{-H}[H^*]$
$\frac{V}{S}\frac{d[D]}{d\tau} = -k_D[D][*] + k_{-D}[D^*]$	$\frac{V}{S}\frac{d[J]}{d\tau} = k_{-J}[J^*]$
$\frac{V}{S}\frac{d[E]}{d\tau} = -k_E[E][*] + k_{-E}[E^*]$	

$\frac{V}{S} = 4.2 \times 10^{-5}$ (cm), where V is the volume of the catalyst bed and S is the total catalyst surface area of the catalyst

Table 7. Rate expressions for adsorbed species in SM2

$\frac{d[A^*]}{d\tau} = k_A[A][*] - (k_{-A} + k_1)[A^*]$	$\frac{d[F^*]}{d\tau} = k_F[F][*] + k_3[C^*] - (k_{-F} + k_4 + k_8)[F^*]$
$\frac{d[B^*]}{d\tau} = k_B[B][*] + k_1[A^*] + k_{-2}[C^*] - (k_{-B} + k_2)[B^*]$	$\frac{d[G^*]}{d\tau} = k_G[G][*] + k_4[F^*] - (k_{-G} + k_5)[G^*]$
$\frac{d[C^*]}{d\tau} = k_C[C][*] + k_2[B^*] - (k_{-C} + k_{-2} + k_3 + k_6 + k_9)[C^*]$	$\frac{d[H^*]}{d\tau} = k_H[H][*] + k_5[G^*] + k_{10}[E^*] - k_{-H}[H^*]$
$\frac{d[D^*]}{d\tau} = k_D[D][*] + k_6[C^*] - (k_{-D} + k_7)[D^*]$	$\frac{d[J^*]}{d\tau} = k_7[D^*] + k_8[F^*] - k_{-J}[J^*]$
$\frac{d[E^*]}{d\tau} = k_E[E][*] + k_9[C^*] - (k_{-E} + k_{10})[E^*]$	

The total concentration of adsorption sites, L, is given as follows:

$$L = \frac{CO\ uptake}{Surface\ area\ of\ catalyst} = \frac{38\ \mu mol\ g^{-1}}{524\ m^2\ g^{-1}}\left(\frac{10^{-4}\ cm^2}{m^2}\right) = 7.3 \times 10^{-6} \mu mol\ cm^{-2}$$

$$L = [*] + [A^*] + [B^*] + [C^*] + [D^*] + [E^*] + [F^*] + [G^*] + [H^*] + [J^*]$$

Fig. 5 shows the fitting results of SM2, along with the experimental results of contact time presented earlier (Fig. 2). The simulated selectivities to 2,3-dihydrobenzofuran and 2-ethylphenol match the experimental values more closely than M1 and M2 and those to the other products also show notable improvements. For instance, the simulated results of toluene and phenol approach the same end values at a contact time of around 0.7 s, instead of the monotonous increase observed with M1 and M2. The fit to the selectivity to ethylbenzene is in good agreement with the experimental points in the entire contact time region, and the results of benzene, 2-ethylcyclohexanol, and ethylcyclohexane continue to show excellent agreement with the experimental data. The R^2 value for SM2 fits was 0.874, an appreciable improvement over the value for the M2 fit (0.809), indicating that SM2 describes the physical situation more accurately.

Table 8. Reaction rate constants obtained for SM2

Adsorption rate const (cm^3 µmol^{-1} s^{-1})		Desorption rate constant (s^{-1})		Reaction rate constant (s^{-1})	
k_A	49	k_{-A}	47	k_1	4.7
k_B	131	k_{-B}	452	k_2	520
k_C	36	k_{-C}	15	k_{-2}	847
k_D	44	k_{-D}	131	k_3	1.9
k_E	2838	k_{-E}	5375	k_4	0.2
k_F	83	k_{-F}	25	k_5	0.56
k_G	7589	k_{-G}	2880	k_6	28
k_H	494	k_{-H}	4710	k_7	1 x 10^{-6}
		k_{-J}	0.048	k_8	155
				k_9	41
				k_{10}	80

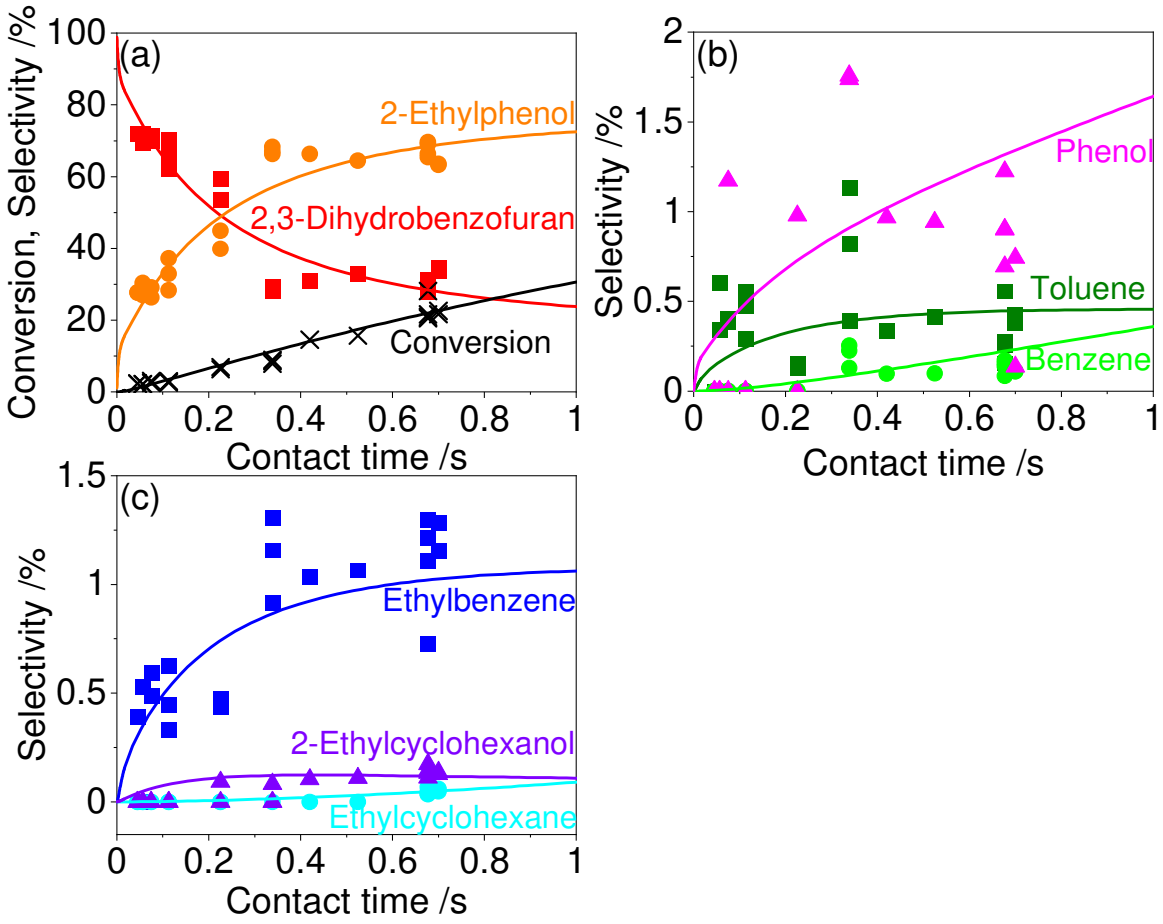

Figure 5. Experimental results (points) of contact time measurement of HDO of benzofuran at 0.5 MPa and 350 °C and calculated fits using SM2 (continuous lines). (a) Conversion of benzofuran and product selectivity for 2,3-dihydrobenzofuran and 2-ethylphenol. (b) Product selectivity for toluene, phenol, and benzene. (c) Product selectivity for ethylbenzene, 2-ethylcyclohexanol, and ethylcyclohexane.

Table 8 and Fig. 4 show adsorption, desorption, and reaction rate constants for surface intermediates obtained from the fitting of SM2. The adsorption rate constants are shown in red on the right of the vertical arrows (Fig. 4) and reveal some interesting behavior. The constant for benzofuran (k_A = 49 cm^3 mol^{-1} s^{-1}) is lower than that for 2,3-dihydrobenzofuran (k_B =131 cm^3 mol^{-1} s^{-1}) which could be related to donation of electron density from the C=C π bond in the furan ring of benzofuran to the catalyst. The adsorption constant for 2-ethylphenol (k_C = 36 cm^3 mol^{-1} s^{-1}) is also lower than that for phenol (k_E = 2838 cm^3 mol^{-1} s^{-1}) which could be due to steric

hindrance to adsorption on the catalyst [66]. The desorption rate constants are shown on the left of the vertical arrows but do not reveal any systematic behavior. The rate constants of the surface reactions are shown in blue with horizontal arrows. From these values alone, it is difficult to deduce the rate-determining step. Previous studies of other cyclic model compounds on supported Ni_2P catalysts indicated that ring-opening step was rate determining [67,68], but this does not appear to be the case here. As shown, the rate constant of the ring-opening step (k_2) was large compared to the rest of the rate constants, which could be an innate property of the bimetallic CoPd phosphide catalyst. Comparison of other rate constants also gives a good picture of the working catalyst. For example, the formation rate of adsorbed ethylbenzene (k_3 = 1.9 s^{-1}) was the highest of the three pathways for the surface transformation of adsorbed 2-ethylphenoxide, an indication that direct deoxygenation was preferred to ring hydrogenation and C-C cracking on this catalyst. The subsequent reaction of adsorbed ethylbenzene to adsorbed toluene (k_9 = 41 s^{-1}), benzene (k_{10} = 80 s^{-1}), and ethylcyclohexane (k_8 = 155 s^{-1}) species is consistent with the observation of these compounds as the main deoxygenated products. The mode of adsorbate bonding is related to the reaction pathway [69] and the suggested steps are reasonable.

Further calculations are presented in the SI that show that the rate constants have values that are physically realistic. In the following, adsorption equilibrium constants calculated from adsorption and desorption rate constants in Table 8 are shown to have values that are physically plausible. This is done by using known values for pre-exponential factors for the general types of reaction considered, and from these calculating the heats of adsorption and showing that they are reasonable.

Particular attention is placed on the equilibrium constants for toluene (G) and benzene (H) which have very different values of the adsorption and desorption constants. For toluene $K(tol) = k_{for}/k_{rev} = 7589/2880 = 2.6$ cm^3 µmol^{-1} and for benzene $K(benz) = k_{for}/k_{rev} = 494/4710 =$ 0.10 cm^3 µmol^{-1}. A typical pre-exponential factor for an adsorption rate constant has a value of $<10^4$ cm s^{-1} and for a desorption rate constant a value of $<10^{28}$ molec cm^{-2}s^{-1} or $< 1.7 \times 10^{10}$ µmol cm^{-2}s^{-1} [70]. The adsorption equilibrium constants are given as the ratio of adsorption and desorption rate constants, $K = k_{for}/k_{rev} = (A_{for}/A_{rev})\exp[(E_{rev}-E_{for})/RT] =$ $(10^4$ cm s$^{-1}/1.7 \times 10^{10}$ µmol cm^{-2} s^{-1}) exp(-ΔH/RT) = 5.9 x 10^{-7} cm^3 µmol^{-1} exp(-ΔH/RT). The adsorption enthalpy is obtained from $\Delta H = E_{for} - E_{rev}$. From these values the adsorption enthalpy for toluene and benzene can be calculated to be ΔH(tol) = -79 kJ mol^{-1} and ΔH(benz) = -62 kJ mol^{-1}. The magnitudes of these heats are physically realistic [71] and to have the heat of toluene be larger than benzene is reasonable.

The analysis of the detailed reaction scheme allows the calculation of coverages of the adsorbates (Fig. 6). The coverages (θ) were calculated from the surface concentrations of the adsorbates ($[A^*]$ and $[P_i^*]$) and the total concentration of adsorption sites (L) according to equation (11).

$$\theta = \frac{[A^*]}{L} \; or \; \frac{[P_i^*]}{L} \tag{11}$$

Recall from Table 7 that L was calculated to be 7.3×10^{-6} µmol cm^{-2}. Fig. 6 shows that the most abundant surface species is adsorbed benzofuran at levels of coverage ranging from 0.48 to 0.68. These values are more than 5 times higher than the second most abundant species (2,3-dihydrobenzofuran and 2-ethylphenol) and substantially higher than that of all other surface intermediates. The predominance of adsorbed benzofuran on the catalyst surface is reasonable and consistent with its low desorption and reaction rate constants. The low coverages of the

aromatic hydrocarbons (benzene, toluene, and ethylbenzene) are in line with these compounds being the main deoxygenated products. Fig. 6 also shows that equilibrium with total site coverage is reached quickly, which is evidenced by the unchanging empty adsorption sites on the catalyst.

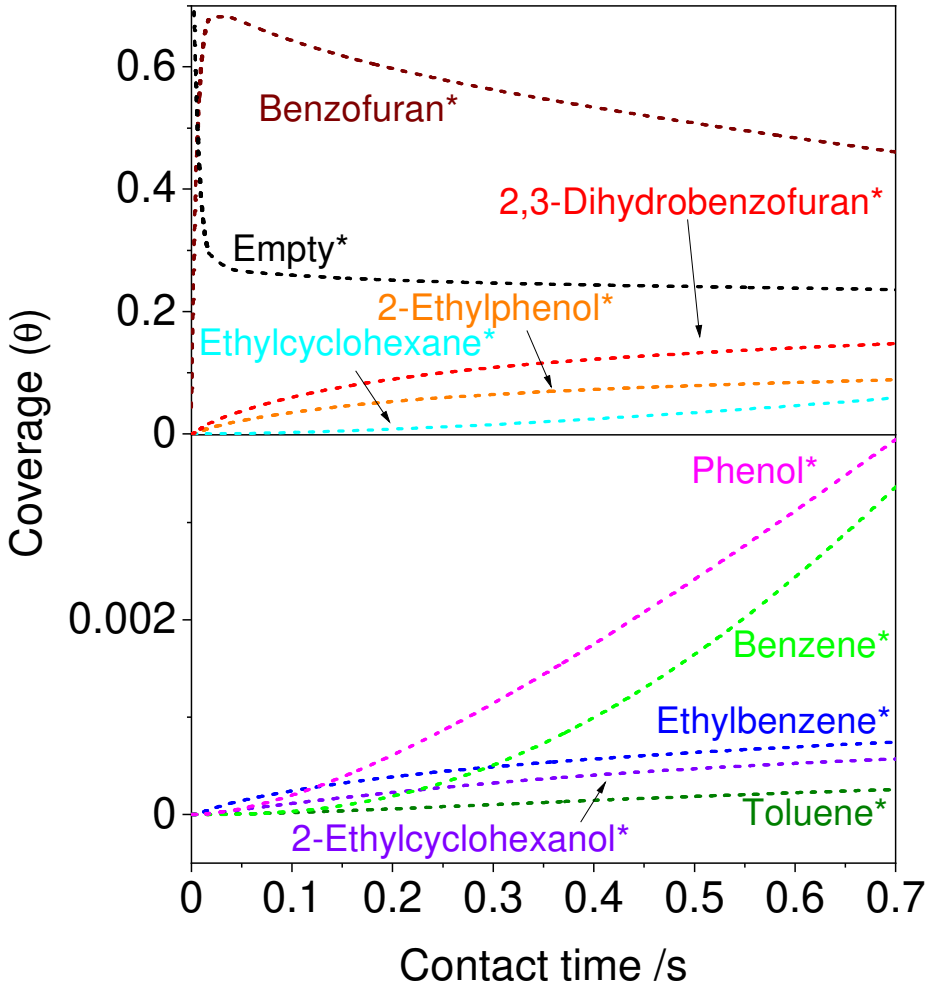

Figure 6. Coverage of adsorbed species as a function of contact time calculated using SM2.

An important consideration when comparing M1, M2, and SM2 is whether the number of fitting parameters play a role in the results. The number of parameters used (in the form of rate constants) in the M1, M2, and SM2 analyses were 10, 11, and 28, respectively, showing a

nearly three-fold increase of parameters from M2 to SM2. This is expected to increase the goodness of fit, regardless of their physical significance. For this reason, the F-test statistic was used to determine whether the increase in the number of parameters were statistically significant. (A description is given in the Experimental Section.) Table 9 shows the results of the F-test on M2 vs M1 (whether the increased number of parameters in M2 is statistically relevant compared to M1), SM2 vs M1, and SM2 vs M2. The residual sum squared (RSS) error is calculated for each test on the 152 data points (value for n) taken during the test. The value p represents the number of parameters (rate constants) used in each model. The R^2 value for each model is included in this table for reference and is not used in calculations for the F-test. For M2 vs M1, the calculated F-factor is 45.8, which is more than 10 times larger than the critical value of 3.91. SM2 vs M1 yields an F-factor of 6.92 that is over 3 times the critical value of 1.60. SM2 vs M2 had a much lower F-factor of 2.81 but is still significantly larger than the critical value of 1.70. The calculated F-test values being higher than the 0.05 critical values indicates that the inclusion of additional parameters in M2 and SM2 are not skewing the results in favor of these models. This shows that accounting for adsorption of species onto the catalyst surface is important for modeling this reaction.

Table 9. F-test on models used for fitting contact time analysis data

	M1 (Fig. S3d)	M2 (Fig. 3d)	SM2 (Fig. 4)
R^2	0.747	0.809	0.874
RSS	0.426	0.322	0.213
p	10	11	28
n	152	152	152
F-factor	M2 vs M1	SM2 vs M1	SM2 vs M2
Calculated	45.8	6.92	2.81
0.05 Critical Values	3.91	1.69	1.70

As can be seen from the prior analyses, the method of fitting reaction networks to models consisting of a series of first-order steps can reveal pertinent reactivity information. However, the derivation of a plausible sequence could involve painstaking analysis which also requires confirmation by relevant spectroscopic measurements using techniques such as the ACT method to determine if observed intermediates are true reaction intermediates [72]. There is also a simpler method, the Delplot technique, which is purported to produce reaction sequences, and this was carried out to check its effectiveness for the case in which adsorbed intermediates are present.

3.5. Delplot analysis of the experimental and modeling results

The reaction sequence of the HDO of benzofuran on CoPd(9:1)P/KUSY was investigated by the Delplot method. This method was first reported by Klein and collaborators [11,12] and has been applied to many types of reactions [73,74,75,76] by construction of plots involving conversion (X) and product yields. In the present case, selectivity (S) or yield/conversion is used to obtain the rank (primary, secondary, tertiary, quaternary, etc.) of a given product by plotting S, S/X, S/X^2, and S/X^3 versus X.

Fig. 7 compares the Delplot analysis of the experimental points with that of the model M2 simulation results. The key result to watch for is the presence of a finite y-axis intercept. For the experimental points, extrapolation of the curves to zero conversion gives ambiguous or inconclusive results because there are no points at sufficiently low conversion, even though points are taken to a level of 2% which gives a lot of noise in the data. Thus, all product curves

appear to have finite intercepts, which does not allow distinguishing their rank (order in the sequence).

For the fitting data of model M2 the results are completely different from the experimental data and give definitive conclusions. The first-rank Delplot shows that only 2,3-dihydrobenzofuran possesses a positive y-intercept, indicating that it is the sole primary product. The second-rank Delplot shows that 2-ethylphenol has a non-zero intercept, indicating that it is a secondary product, whereas 2,3-dihydrobenzofuran has a diverging intercept, consistent with its assignment as a primary product. Furthermore, the other products have zero y-intercepts, suggesting that they appear later in the sequence. The third-rank Delplot shows that phenol, ethylbenzene, and 2-ethylcyclohexanol have finite y-intercepts which indicate that they are tertiary products, and finally the fourth-rank Delplot shows that toluene, benzene, and ethylcyclohexane have non-zero y-intercepts and thus are quaternary (final) products. The identified sequence is self-consistent with the proposed scheme of Fig. 3d. Thus, this result suggests that a means of utilizing the Delplot method for gas-phase species when experimental points are limited is to fit the data to a model and use the resulting low conversion values to determine if the predicted ranks agree with the model.

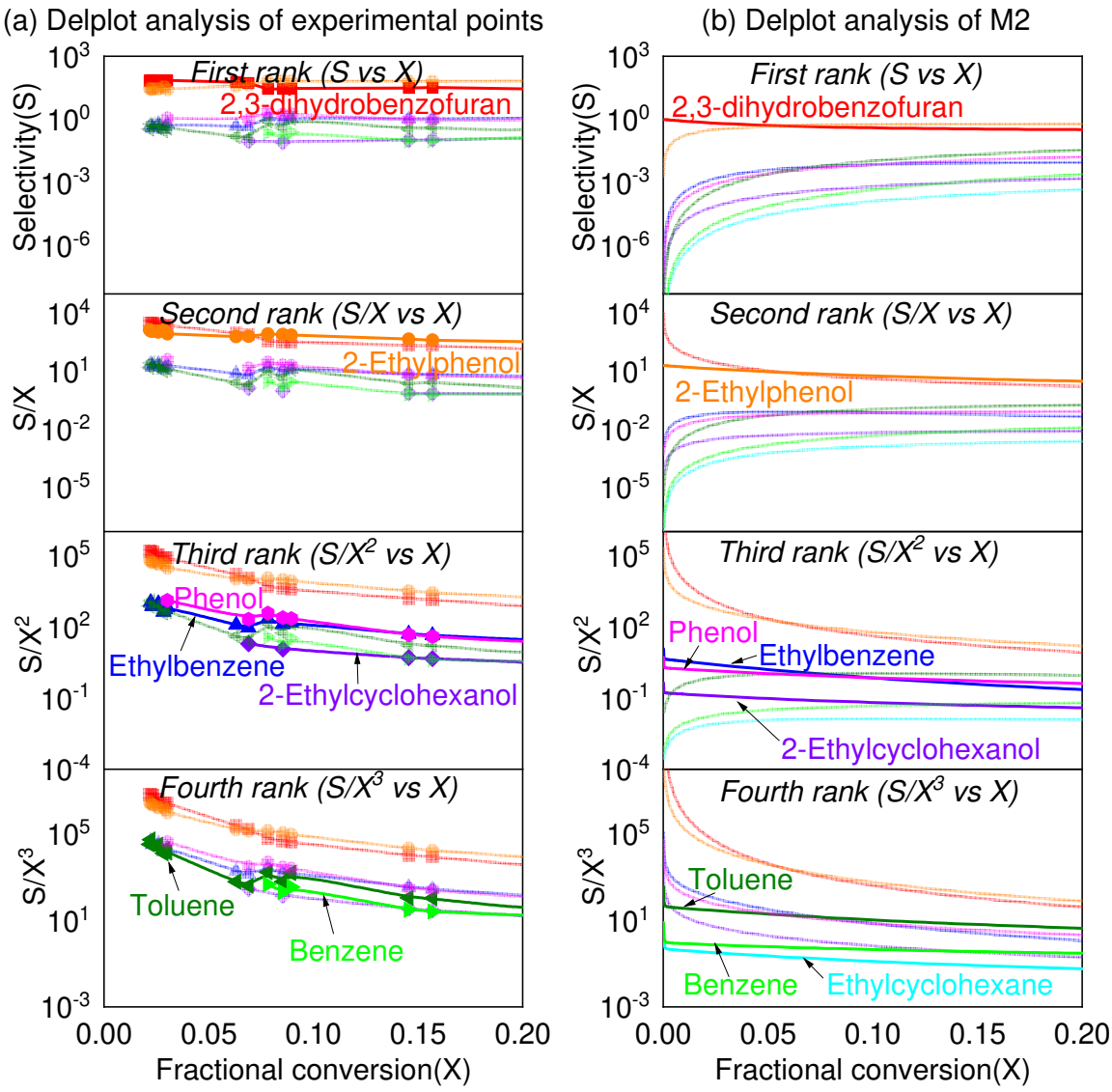

Figure 7. Delplot analysis of the HDO of benzofuran on CoPd(9:1)P/KUSY at 0.5 MPa and 350 °C with (a) the experimental points and (b) the fitting results of M2.

A Delplot analysis of M1 was also carried out and is shown in the SI section. Thus, Delplot analyses for both M1 and M2 show excellent agreement with the proposed simple reaction networks (M1 and M2) and give them support. The results also show that the existence of a reversible step in the scheme of M2 did not affect deductions from the Delplot analysis. Previous work on Delplot analysis showed that the magnitude of rate constants was important in

determining a sequence of a reaction [77] and, thus, the identical sequence obtained for M1 and M2 could be due to similarities of the rate constants of that second step.

Fig. 8 shows the Delplot analysis of the fitting results of SM2. This is a kinetic modeling with a rake mechanism, and Delplot analyses of both the gaseous species and adsorbed intermediates were carried out. For the gaseous species (Fig. 8a), the analysis indicates that 2,3-dihydrobenzofuran is a primary gaseous product (first-rank, S vs X), while benzene and ethylcyclohexane are secondary products (second-rank, S/X vs X). Although the first-rank Delplot is in accordance with the sequential network of SM2, the second-rank Delplot is not. Furthermore, the third- and fourth-rank Delplots did not show any finite intercepts. For the surface species (Fig. 8b), the result shows that benzofuran is the primary adsorbate (first-rank, S vs X), and toluene, 2-ethylcyclohexanol, and phenol are secondary adsorbates (second-rank, S/X vs X). Similarly, there were no identified subsequent products. These results are inconsistent with the network of Fig. 4, which is surprising because, as previously shown, analysis of the sequence with adsorbates gave the most accurate description of the reaction. It is difficult to speculate about the origin of the inconsistency as there are no precedents of Delplot analysis with adsorbed intermediates. A previous study of Delplot analysis without adsorbates revealed that an overly large rate constant in a step in the sequence was responsible for the lack of applicability of higher rank Delplots to contact time results [78]. As will be discussed later, the magnitude of adsorption equilibrium constants appears to strongly affect the Delplot analysis with adsorbates.

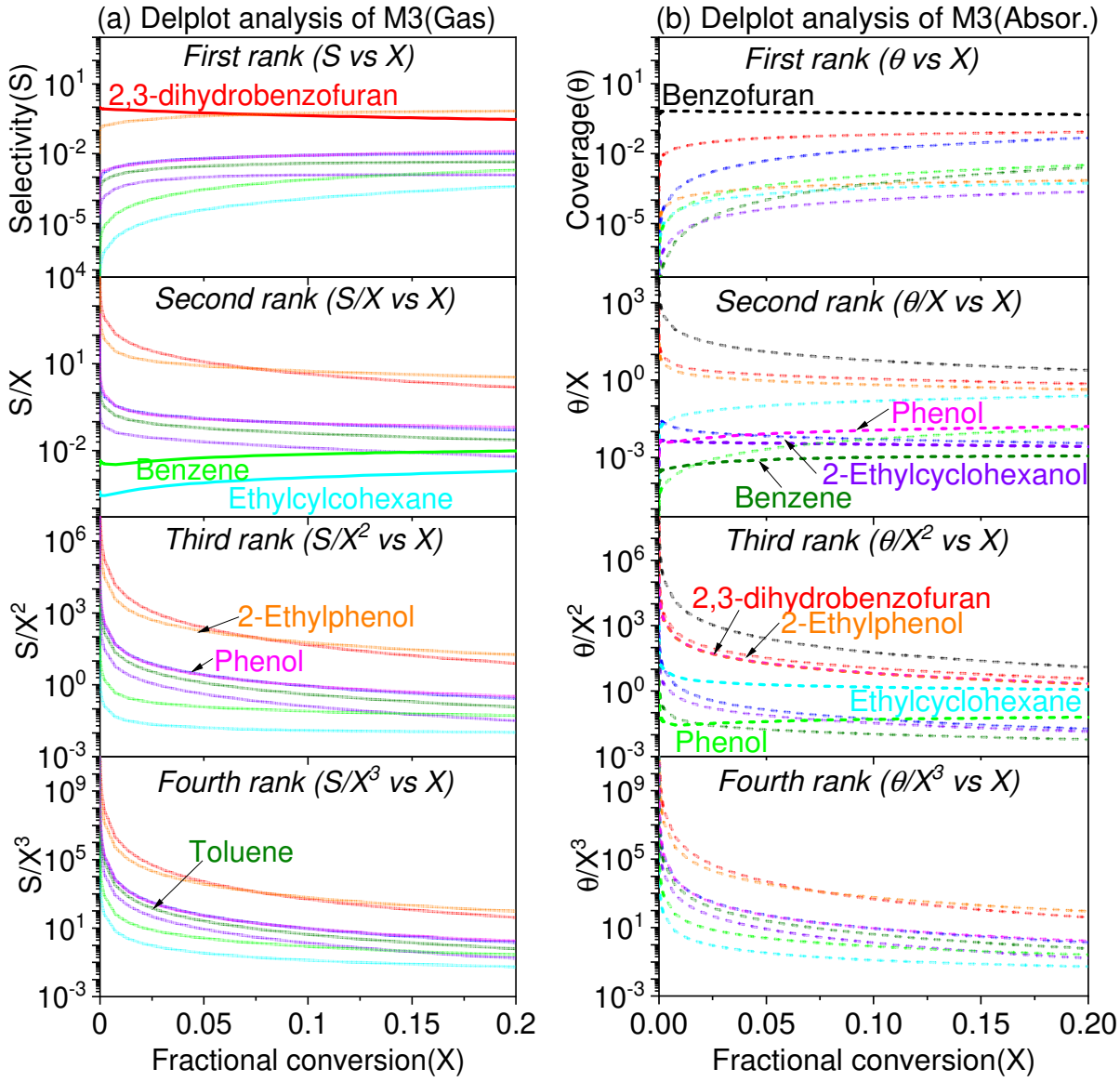

Figure 8. Delplot analysis of fitting results (SM2) of the HDO of benzofuran on CoPd(9:1)P/KUSY at 0.5 MPa and 350 °C (a) for gaseous species and (b) for adsorbed species.

3.7. Delplot analysis of a model sequence

The explanation for why the Delplot analysis does not work for a reaction network with adsorbates is important to examine its applicability to comprehensive networks consisting of

elementary steps. Subsequent Delplot analysis studies by Klein and coworkers dealing with products of multiple ranks [20], non-isothermal conditions [21], reaction reversibility [22], and reaction mechanisms with varying rate constants [23] have indicated that the method is not generally applicable in a number of cases, such as networks with large differences in the magnitude of rate constants. For the present study involving both gas-phase species and adsorbates, it is of interest to examine whether large rate constants for adsorption and desorption were responsible for the inapplicability of the method. A simulation of a model sequence is used to investigate the influence of the rate constants for adsorption and desorption on the deduction of a reaction sequence and is discussed below.

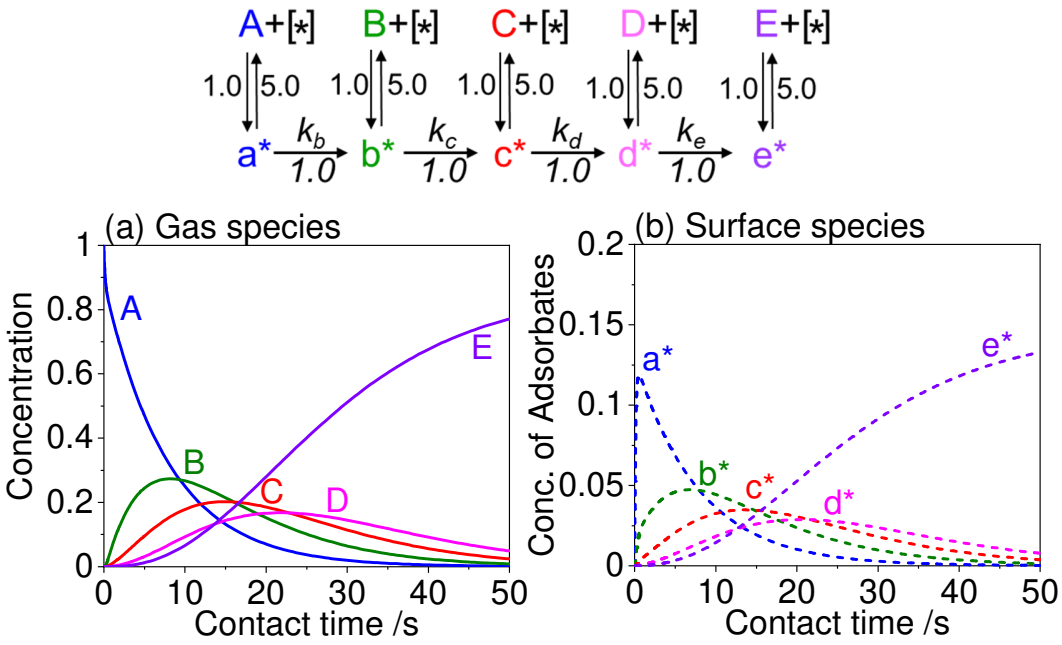

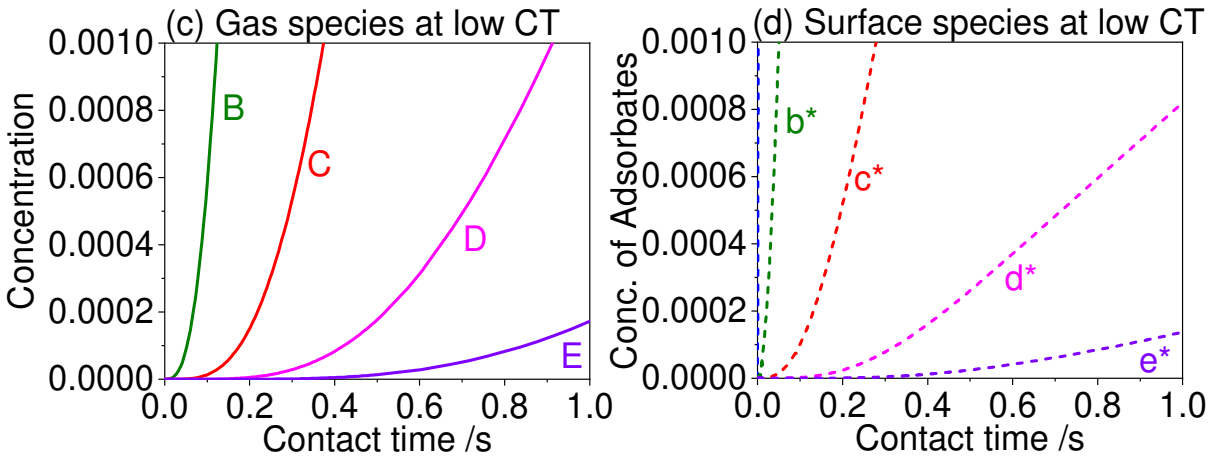

Figure 9 Analytical solutions for the illustrated sequence. (a) Gas phase species, (b) Surface species, (c) Gas-phase species at low contact time (CT), (d) Surface species at low contact time (CT) Assumed rate constants (k_b, k_c, k_d, k_e = 1.0 s^{-1}), adsorption constants (1.0 cm^3 μmol^{-1} s^{-1}), and desorption constants (5.0 s^{-1}) were the same for each step.

Fig. 9 shows an analytical solution for a sequential network with adsorbates and with assumed rate constants all equal to 1.0 s^{-1}, adsorption constants all equal to 1.0 cm^3 μmol^{-1} s^{-1}, and desorption constants all equal to 5.0 s^{-1}. Fig. 9a shows the concentration of the gaseous species as a function of contact time and is consistent with the expected sequence. The reactant A shows a nonzero concentration at zero contact time that decreases with increasing contact time. The products B, C, and D initially show zero concentrations which go through maxima and then decrease, behavior characteristics of intermediate products. The order of appearance of the maxima is B (primary product), C (secondary product), and D (tertiary product). The product E also initially shows zero concentration but increases steadily with contact time, consistent with a final product. Fig. 9b shows the concentration profiles of the adsorbed intermediates which also reflect the trend observed in the scheme. Figs. 9c and d show an expanded view in the low contact time region of the concentration profiles. Comparison of these figures to others to be shown later reveal differences that are not observable in the wide contact time region.

Fig. 10a shows a model Delplot fitting of the gaseous species for the sequential sequence of Fig. 9 (top). The first, second, third, and fourth rank Delplots show finite intercepts for B, C, D, and E, respectively. Fig. 10b shows the corresponding model Delplot fitting of the surface species. Similarly, the first, second, third, and fourth rank Delplots show finite intercepts for b^*, c^*, d^*, and e^*, respectively. In addition, the analyses show appropriate zero and divergent intercepts for the relevant species. The results are consistent with the scheme shown in Fig. 9 (top), namely, B, C, D, and E as the primary, secondary, tertiary, and final gaseous product, respectively, and b^*, c^*, d^*, and e^*, as the primary, secondary, tertiary, and final surface species, respectively. This confirms that the Delplot method functions well for a reaction sequence with adsorbates when the rate constants and equilibrium adsorption constants do not differ substantially.

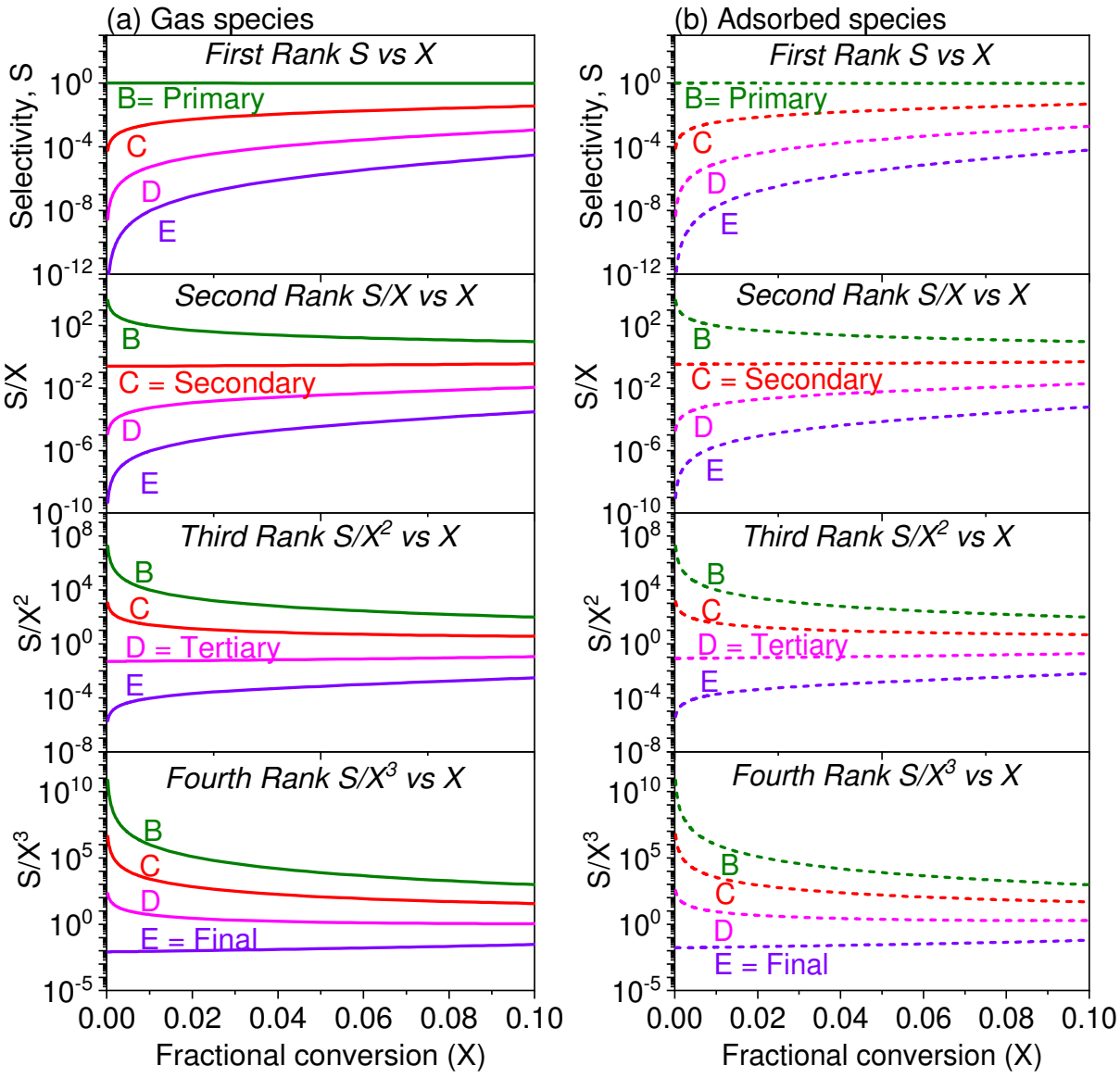

Figure 10. Delplot analysis for the sequential sequence of Fig. 9 in which assumed rate constants (1.0 s^{-1}), adsorption constants (1.0 cm^3 μmol^{-1} s^{-1}), and desorption constants (5.0 s^{-1}) were the same for each step (a) for gaseous species and (b) for adsorbed species.

Fig. 11 shows another analytical solution for a sequential sequence with adsorbates in which the assumed rate constants for all the steps are equal, and the adsorption and desorption constants for all but one of the steps are equal. A step with an overly large equilibrium constant

was included in the sequence because the scheme of Fig. 4 includes such a step (e.g. the adsorption/desorption of toluene step). The concentration profiles of the gaseous species (Fig. 11a) and adsorbates (Fig. 11b) are consistent with the sequence of reaction steps (Fig. 11 (top)). The curves shown here are identical to the analogous curves shown in Fig. 9, suggesting that the large adsorption/desorption constants do not affect the concentrations substantially. They also suggest, that there is no change in the reaction orders of the steps, which were assumed to be first-order. However, an expanded view of the curves in the low contact time region (Figs. 9c and 9d versus Figs. 11c and 11d) reveal some subtle distinctions. The most notable are the slopes of the concentrations of the adsorbed species d (d*) and e (e*) and gaseous species E. In the present case with larger adsorption/desorption constants, the concentrations increase less sharply compared to the previous case. This causes the deviations in the Delplot asymptotes at low contact times.

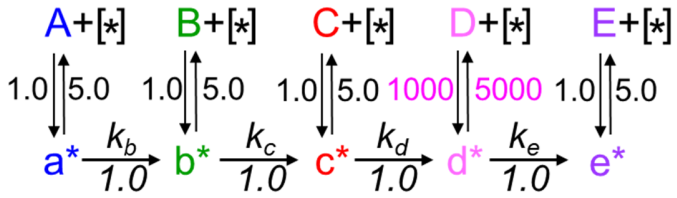

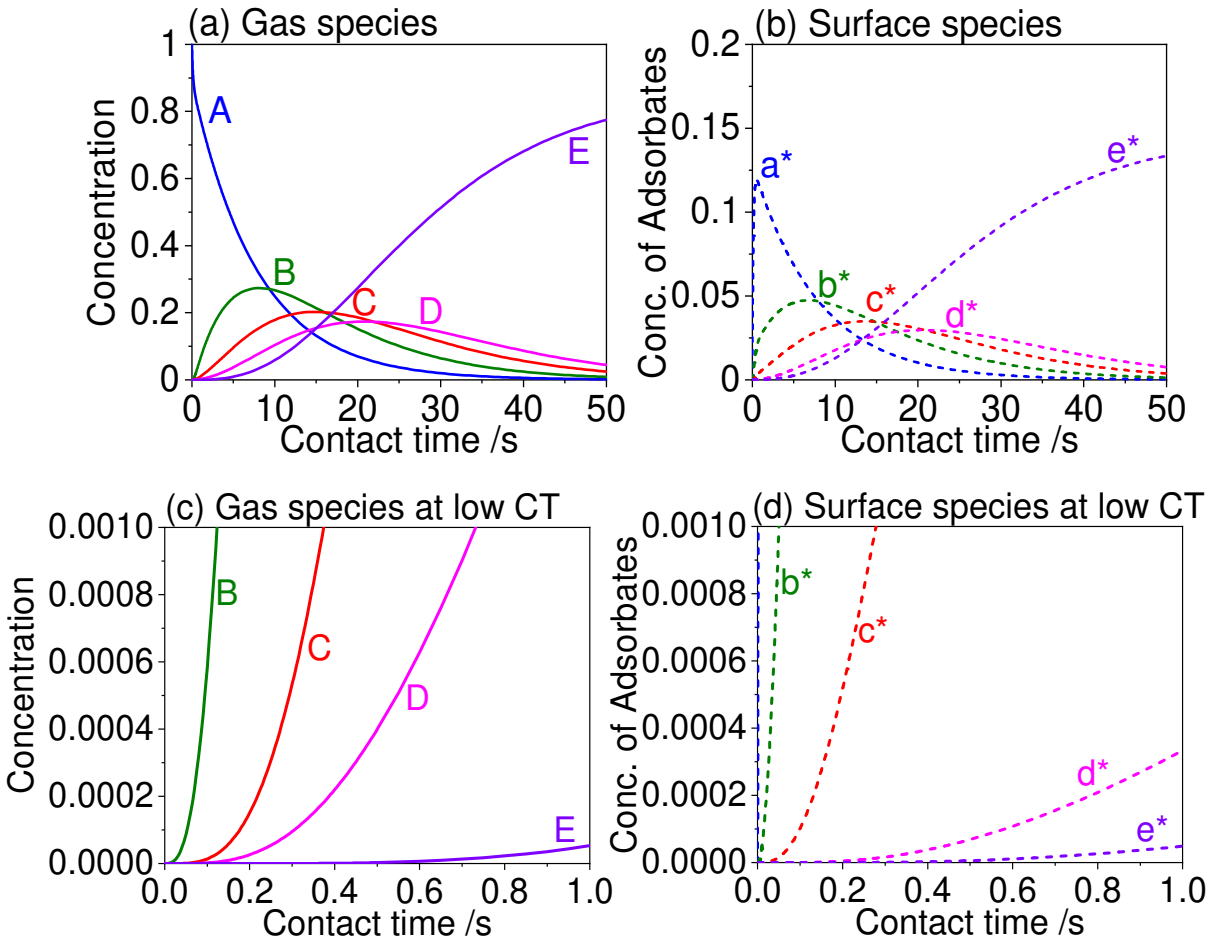

Figure 11. the illustrated sequence. (a) Gas phase species, (b) Surface species, (c) Gas-phase species at low contact time (CT), (d) Surface species at low contact time (CT) The assumed rate constants (k_b, k_c, k_d, k_e = 1.0 s^{-1}) were the same for each step, whereas adsorption constants (1.0 cm^3 μmol^{-1} s^{-1}) and desorption constants (5.0 s^{-1}) were the same for all but one step (adsorption constant =1000 cm^3 μmol^{-1} s^{-1} and desorption constant = 5000 s^{-1}).

Fig. 12a shows a model Delplot fitting of the gaseous species for the sequential sequence of Fig 11 (top) and Fig. 12b shows the Delplot fitting for the surface species. The plots are very similar to those of Fig. 10, but differ subtly in the short contact time region. The results for the first, second, and fourth rank Delplots are in accordance with the order of appearance of the respective species in the sequence: B as the primary product, C as the secondary product, and E as the final product. In contrast, the third rank Delplot indicates that there are no tertiary products,

with the analysis instead showing a diverging intercept for the expected tertiary gaseous species (D). Fig. 12b shows that the Delplot fitting of the adsorbed intermediates exhibits the same characteristics as the gas-phase counterparts. The anomalous behavior of the species D and d^* from the third-rank Delplot analysis is clearly related to the large constants, as the species desorbs more rapidly and, thus, display features similar to species in preceding steps. These results suggest that the successful application of the Delplot method to networks with adsorbed species is contingent on the existence of reaction steps with comparable surface reaction and adsorption/desorption constants.

Interestingly, the lack of applicability of the Delplot method does not apply to standard methods of plotting concentration versus contact time as shown by the almost identical plots in Figs. 9 and 11. Since the concentrations can readily be converted to selectivities, this means that the most reliable method of determining a reaction sequence is by plotting selectivities versus contact time. Selectivities allow easy identification of primary intermediates because since they are formed first these alone extrapolate to 100% at zero conversion. This is different from concentrations or yields in which all product species start at zero. In addition, the order of the species in the sequence can be determined by the order of appearance of peaks (B → C → D in Figs. 9a and 11a), the initial slopes (B finite, C and D zero), and the curve shapes (E rising).

It is also of interest to consider what happens when one of the rate constants (k_b, k_c, k_d, or k_e) takes on a substantially greater value than the rest. This was actually analyzed in a previous publication where adsorbates were not considered [78], and the results showed that the Delplot method could not predict the reaction sequence. The case here with adsorbates is considered in the SI section and it is found that when a rate constant is changed by a factor of 1000 a perturbation of the Delplot analysis starts to be discernible and when it is changed by a factor of

10,000 the Delplot method ceases to be applicable. The findings here are consistent with previous reports by Klein and coworkers that network information by the Delplot method can be obscured by the magnitude of rate constants [20, 23].

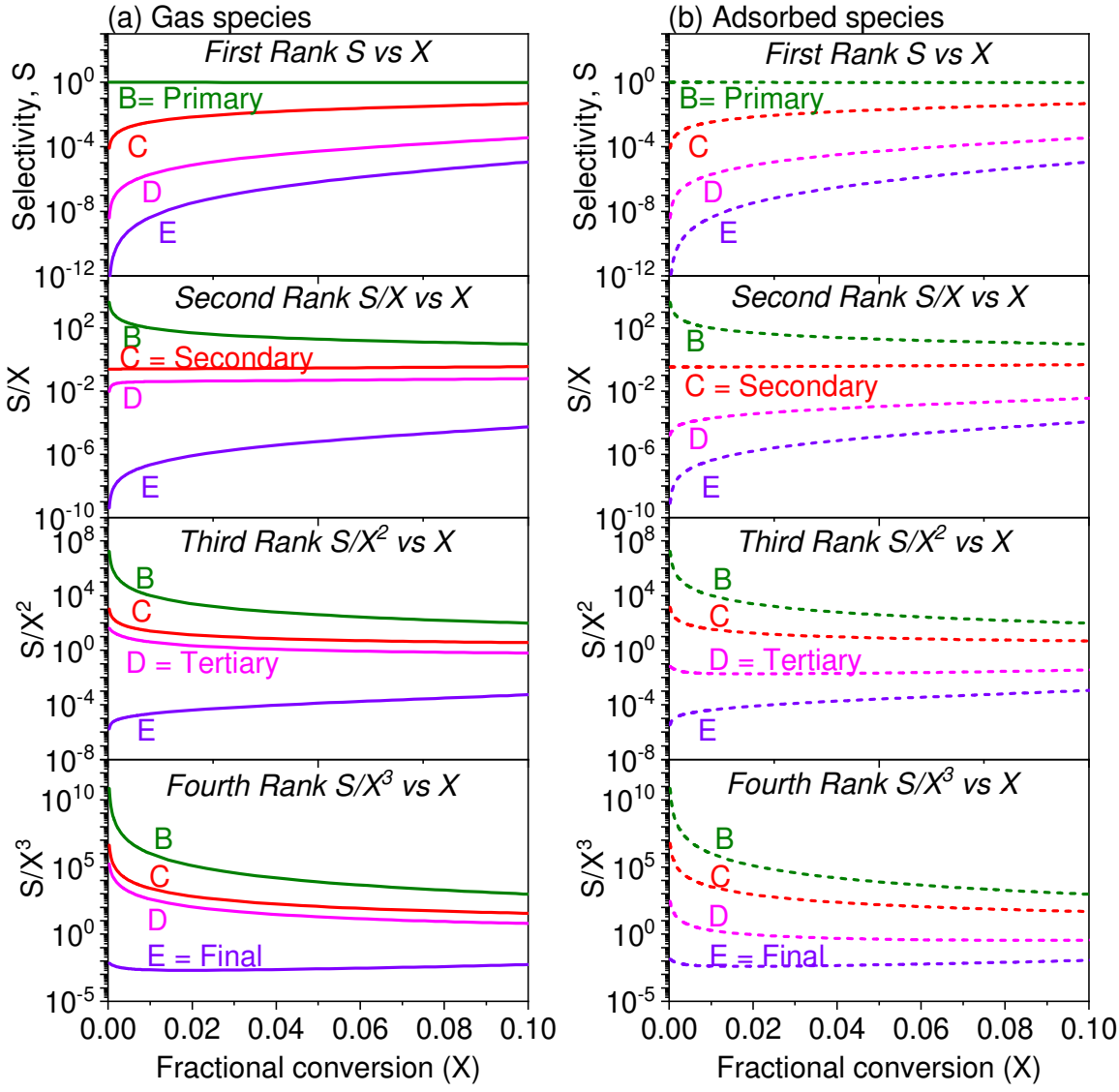

Figure 12. Delplot analysis for the sequential sequence of Fig. 11 in which assumed rate constants (k_b, k_c, k_d, k_e = 1.0 s^{-1}) were the same for each step, whereas adsorption constants (1.0 cm^3 μmol^{-1} s^{-1}) and desorption constants (5.0 s^{-1}) were the same for all but one step (adsorption constant =1000 cm^3 μmol^{-1} s^{-1} and desorption constant = 5000 s^{-1}) (a) for gaseous species and (b) for adsorbed species.

Although it is an important finding that the Delplot analysis agrees with the simple non-adsorbate networks, it is a significant limitation that it does not work for the more comprehensive sequence with adsorbates. This suggests that Delplot analysis can miss essential steps in the reaction pathway because it is impossible to know a priori the kinetic constants and the chemistry of each of the steps.

4. Conclusions

A combination of contact time measurements, kinetic modeling, and Delplot analyses was used to investigate the HDO of benzofuran on a supported bimetallic CoPd phosphide catalyst at 0.5 MPa and 350 °C. Eight types of reaction networks were analyzed, four simple ones involving only the observed gas-phase species and four analogous detailed network considering adsorbed species. The following conclusions can be obtained.

1) Analysis of products of reaction as a function of contact time can be used to obtain reaction sequences.
2) The best contact time for kinetic studies is one based on the number of sites.
3) Consideration of surface species gives more accurate descriptions of reaction sequences and higher regression coefficients.
4) The Delplot method of plotting the ratios of selectivity to various powers of the conversion works for the simple models and predicts the primary, secondary, tertiary and final products (species rank).
5) The Delplot method cannot be applied to the more complex models because the presence of overly large rate constants for adsorption causes the species rank to be

misidentified, making the Delplot analysis generally inapplicable for determining sequences involving adsorbed species.

Acknowledgments

This work was supported by the US Department of Energy under grant DE-FG02-96ER14669. WJM acknowledges support from the Tonen International Scholarship Foundation and the University of Tokyo Doctoral Student Special Incentives Program (SEUT-RA). STO acknowledges Fuzhou University as Mingjiang Chair Professor. The EXAFS measurements were performed under the approval of the Photon Factory Program Advisory Committee (Proposal Nos. 2017G083 and 2019G070).

Personal acknowledgment

This paper is dedicated to Michel Boudart, with whom one of us (Ted Oyama) received his doctorate at Stanford University. Professionally, Michel has been a guiding light and a source of inspiration for a lifetime of research in kinetics and mechanism. Personally, Michel and his wife Marina, have been guardian angels who made possible the tying of a lifelong knot between Ted and Hideko.

References

[1] M. Boudart, Kinetics of Chemical Processes, Prentice Hall, Englewood Cliffs, New Jersey, 1968, p. 210.

[2] M. Boudart, From the century of the rate equation to the century of the rate constants: a revolution in catalytic kinetics and assisted catalyst design, Catal. Lett. 65 (2000) 1-3.

[3] M. Boudart, Turnover rates in heterogeneous reactions, Chem. Rev. 95 (1995) 661-666.

[4] M. Boudart, Perspectives in Catalysis, Blackwell Scientific Publications, Oxford, 1992, p. 183

[5] M. Boudart, G. Djèga-Mariadassou, Kinetics of heterogeneous catalytic reactions, Princeton Univ. Press, Princeton, New Jersey, 1984, pp. 108-116.

[6] Froment, G. F.. and Bischoff, K. B., "Chemical Reactor Analysis and Design." Wiley, New York, 1979.

[7] K. J. Laidler, Chemical kinetics, 3rd Ed., Harper & Row, New York, 1987, pp. 278-281.

[8] E. Vynckier, G. Froment, Modeling of the kinetics of complex processes based upon elementary steps, in: G. Astarita, S. Sandler (Eds.), Kinetic and Thermodynamic Lumping of Multicomponent Mixtures, Elsevier B.V., Amsterdam, 1991, pp. 131−161.

[9] M.A. Gonzalez-Borja, D.E. Resasco, Anisole and guaiacol hydrodeoxygenation over monolithic Pt-Sn Catalysts, Energy & Fuels 25 (2011) 4155-4162.

[10] M.V. Bykova, D.Y. Ermakov, V.V. Kaichev, O.A. Bulavchenko, A.A. Saraev, M.Y. Lebedev, V.A. Yakovlev, Ni-based sol–gel catalysts as promising systems for crude bio-oil upgrading: Guaiacol hydrodeoxygenation study, Appl. Catal. B: Env. 113 (2012) 296-307.

[11] N.A. Bhore, M.T. Klein, K.B. Bischoff, The Delplot technique: A new method for reaction pathway analysis, Ind. Eng. Chem. Res. 29 (1990) 313-316.

[12] N.A. Bhore, M.T. Klein, K.B. Bischoff, Species rank in reaction pathways: Application of Delplot analysis, Chem. Eng. Sci. 45 (1990) 2109-2116.

[13] Y. K. Chow, N. F. Dummer, J. H. Carter, R. J. Meyer, R. D. Armstrong, C. Williams, G. Shaw, S. Yacob, M. M. Bhasin, D. J. Willock, S. H. Taylor, G. J. Hutchings, Kinetic study of methane partial oxidation over Fe-ZSM-5 using N_2O as an oxidant, ChemPhysChem 19 (2018) 402-411.

[14] H. Wei, C. Gomez, J. Liu, N. Guo, T. Wu, R. Lobo-Lapidus, C.L. Marshall, J.T. Miller, R.J. Meyer, Selective hydrogenation of acrolein on supported silver catalysts: A kinetics study of particle size effects, J. Catal. 298 (2013) 18-26.

[15] T. Rajkhowa, G.B. Marin, J.W. Thybaut, A comprehensive kinetic model for Cu catalyzed liquid phase glycerol hydrogenolysis, Appl. Catal. B 205 (2017) 469-480.

[16] C.A. Badari, F. Lónyi, E. Drotár, A. Kaszonyi, J. Valyon, A study of the hydrodenitrogenation of propylamine over supported nickel phosphide catalysts using amorphous and nanostructured silica supports, Appl. Catal. B 164 (2015) 48-60.

[17] I.T. Ghampson, R. Canales, N. Escalona, A study of the hydrodeoxygenation of anisole over Re-MoO_x/TiO_2 catalyst, Appl. Catal. A 549 (2018) 225-236.

[18] G. Seonga, M. Dejhosseinia, T. Adschiri, A kinetic study of catalytic hydrothermal reactions of acetaldehyde with cubic CeO_2 nanoparticles, Appl. Catal. A 550 (2018) 284-296.

[19] J.D. Sheehan, A. Abraham, P.E. Savage, Reaction pathways and kinetics for tetra-alanine in hot, compressed liquid water, React. Chem. Eng. 4 (2019) 1237-1252.

[20] M.T. Klein, Z. Hou, C. Bennett, Reaction network elucidation: Interpreting Delplots for mixed generation products, Energy Fuels 26 (2012) 52-54.

[21] N.S. Abo-Ghander, M.T. Klein, Influence of reaction temperature on the interpretation of Delplots for the parallel-series reaction network, Energy Fuels 32 (2018) 10904-10909.

[22] N.S. Abo-Ghander, M.T. Klein, Influence of reaction reversibility on the interpretation of Delplots of the parallel-series reaction network, Energy Fuels 33 (2019) 1444-1449.

[23] N.S. Abo-Ghander, M.T. Klein, Delplot-compliant data: Molecular observables versus reaction intermediates, Energy Fuels 34 (2020) 15443-15447.

[24] A.V. Bridgwater, Review of fast pyrolysis of biomass and product upgrading, Biomass Bioenergy 38 (2012) 68-94.

[25] D. Mohan, C.U. Pittman Jr., P.H. Steele, Pyrolysis of wood/biomass for bio-oil: A critical review, Energy Fuels 20 (2006) 848−889.

[26] E. Furimsky, Catalytic hydrodeoxygenation, Appl. Catal. A: Gen. 199 (2000) 147−190.

[27] E. Taarning, C.M. Osmundsen, X. Yang, B. Voss, S.I. Andersen, C.H. Christensen, Zeolite-catalyzed biomass conversion to fuels and chemicals, Energy Environ. Sci. 4 (2011) 793–804.

[28] J. Zakzeski, P.C.A. Bruijnincx, A.L. Jongerius, B.M. Weckhuysen, The catalytic valorization of lignin for the production of renewable chemicals, Chem. Rev. 110 (2010) 3552-3599.

[29] C. Liu, Z. Shao, Z. Xiao, C.T. Williams, C. Liang, Hydrodeoxygenation of benzofuran over silica–alumina-supported Pt, Pd, and Pt–Pd catalysts, Energy Fuels 26 (2012) 4205-4211.

[30] C. Liu, Z. Shao, Z. Xiao, C. Liang, Hydrodeoxygenation of benzofuran over activated carbon supported Pt, Pd, and Pt–Pd catalysts, React. Kinet. Mech. Cat. 107 (2012) 393-404.

[31] A.Y. Bunch, U.S. Ozkan, Investigation of the reaction network of benzofuran hydrodeoxygenation over sulfided and reduced Ni-Mo/Al_2O_3 catalysts, J. Catal. 206 (2002) 177-187.

[32] A.Y. Bunch, X.Q. Wang, U.S. Ozkan, Hydrodeoxygenation of benzofuran over sulfided and reduced Ni-Mo/γ-Al_2O_3 catalysts: Effect of H_2S, J. Mol. Catal. A: Chem. 270 (2007) 264-272.

[33] Y. Romero, F. Richard, Y. Reneme, S. Brunet, Hydrodeoxygenation of benzofuran and its oxygenated derivatives (2,3-dihydrobenzofuran and 2-ethylphenol) over NiMoP/Al_2O_3 catalyst, Appl. Catal. A 353 (2009) 46-53.

[34] H. Abe, A.T. Bell, Catalytic hydrotreating of indole, benzothiophene, and benzofuran over Mo_2N, Catal. Lett. 18 (1993) 1-8.

[35] H. Song, J. Gong, H. Song, F. Li, A novel surface modification approach for synthesizing supported nickel phosphide catalysts with high activity for hydrodeoxygenation of benzofuran, Appl. Catal. A 505 (2015) 267-275

[36] H.Y. Zhao, D. Li, P. Bui, S.T. Oyama, Hydrodeoxygenation of guaiacol as model compound for pyrlysis oil on transition metal phosphide hydroprocessing catalysts, Appl. Catal. A 391 (2011) 305-310.

[37] D.J. Rensel, S. Rouvimov, M.E. Gin, J.C. Hicks, Highly selective bimetallic FeMoP catalyst for C–O bond cleavage of aryl ethers, J. Catal. 305 (2013) 256-263.

[38] P. Bui, J.A. Cecilia, S.T. Oyama, A. Takagaki, A. Infantes-Molina, H. Zhao, D. Li, E. Rodríguez-Castellón, A. Jiménez-López, Studies of the synthesis of transition metal phosphides and their activity in the hydrodeoxygenation of a biofuel model compound, J. Catal. 294 (2012) 184-198.

[39] J.A. Cecilia, A. Infantes-Molina, E. Rodríguez-Castellón, A. Jiménez-López, S.T. Oyama, Oxygen-removal of dibenzofuran as a model compound in biomass derived bio-oil on nickel phosphide catalysts: Role of phosphorus, Appl. Catal. B. 136–137 (2013) 140-149.

[40] J. Chen, H. Shi, L. Li, K. Li, Deoxygenation of methyl laurate as a model compound to hydrocarbons on transition metal phosphide catalysts, Appl. Catal. B. 144 (2014) 870-884.

[41] T.A. Le, H.V. Ly, J. Kim, S. Kim, J.H. Choi, H. Woo, M.R. Othman, Hydrodeoxygenation of 2-furyl methyl ketone as a model compound in bio-oil from pyrolysis of Saccharina Japonica Alga in fixed-bed reactor, Chem. Eng. J. 250 (2014) 157-163.

[42] A. Iino, A. Cho, A. Takagaki, R. Kikuchi, S.T. Oyama Kinetic studies of HDO of 2-methyl-tetrahydrofuran on a Ni_2P/SiO_2 catalyst, J. Catal. 311 (2014) 17–27.

[43] V.T. da Silva, L.A. Sousa, R.M. Amorim, L. Andrini, S.J.A. Figueroa, F.G. Requejo, F.C. Vicentini, Lowering the synthesis temperature of Ni_2P/SiO_2 by palladium addition, J. Catal. 279 (2011) 88-102.

[44] J.A. Cecilia, A. Infantes-Molina, J. Sanmartín-Donoso, E. Rodríguez-Aguado, D. Ballesteros-Plata, E. Rodríguez-Castellón, Enhanced HDO activity of Ni_2P promoted with noble metals, Catal. Sci. Technol. 6 (2016) 7323-7333.

[45] Y. Li, X. Yang, L. Zhu, H. Zhang, B. Chen, Hydrodeoxygenation of phenol as a bio-oil model compound over intimate contact noble metal-Ni_2P/SiO_2 catalysts, RSC Adv. 5 (2015) 80388-80396.

[46] L.F. Feitosa, G. Berhault, D. Laurenti, T.E. Davies, V.T. da Silva, Synthesis and hydrodeoxygenation activity of Ni_2P/C – Effect of the palladium salt lowering the nickel phosphide synthesis temperature, J. Catal. 340 (2016) 154-165

[47] M. Boudart, G. Djéga-Mariadessou, Kinetics of Heterogeneous Catalytic Reactions, Princeton Univ. Press, Princeton, New Jersey, 1984, Chapter 3, p. 110.

[48] J. P. Wauquier, J.C. Jungers, La cinetique quantitative en catalyse et la selectivite du catalyseur, Bull. Soc. Chim. France 8-9 (1957) 1280-1288.

[49] W.J. Movick, G.-N. Yun, V. Vargheese, K.K. Bando, R. Kikuchi, S.T. Oyama, Hydrodeoxygenation of benzofuran on novel CoPdP catalysts supported on potassium ion exchanged ultra-stable Y-zeolites, J. Catal. (in press) https://doi.org/10.1016/j.jcat.2021.01.023.

[50] Y.-K. Lee, Y. Shu, S.T. Oyama, Active phase of a nickel phosphide (Ni_2P) catalyst supported on KUSY zeolite for the hydrodesulfurization of 4,6-DMDBT, Appl. Catal. A 322 (2007) 191-204

[51] J. Lu, J. J. Bravo-Suárez, M. Haruta, S. T. Oyama, Direct propylene epoxidation over modified Ag/$CaCO_3$ catalysts, Appl. Catal. A: Gen. 302 (2006) 283-295.

[52] S. Fogler, Elements of Chemical Reaction Engineering, Fourth Edition, Prentice Hall, 2005.

[53] C. Stinner, R. Prins and Th. Weber, Binary and ternary transition-metal phosphides as HDN catalysts, J. Catal., 202 (2001) 187-194.

[54] A. De Vylder, J. Lauwaert. S. Van Auwenis. J. De Clercq. J. W. Thybaut, Catalyst stability assessment in a lab-scale liquid-solid $(LS)^2$ plug-flow reactor, Catalysts 9 (2019) 755-772.

[55] J.W. Eaton, D. Bateman, S. Hauberg, R. Wehbring, GNU Octave version 3.8.1 manual: A high-level interactive language for numerical computations, in, CreateSpace Independent Publishing Platform, 2014.

[56] S. Rundqvist, Phosphides of the B31 (MnP) Structure Type, Acta Chem Scand. 16 (1962) 287-292

[57] B. Mierzwa, Z. Kaszkur, B. Moraweck, J. Pielaszek, In situ EXAFS study of the allow catalyst Pd-Co (50%/50%)/SiO_2, J. Alloys Compd. 286 (1999) 93-97.

[58] C.L. Lee, D.F. Ollis, Catalytic hydrodeoxygenation of benzofuran and ortho-ethylphenol, J. Catal. 87 (1984) 325-331.

[59] M.C. Edelman, M.K. Maholland, R.M. Baldwin, S.W. Cowley, Vapor-phase catalytic hydrodeoxygenation of benzofuran, J. Catal. 111 (1988) 243-253.

[60] Y. Romero, F. Richard, S. Brunet, Hydrodeoxygenation of 2-ethylphenol as a model compound of bio-crude over sulfided Mo-based catalysts: Promoting effect and reaction mechanism, Appl. Catal. B 98 (2010) 213-223.

[61] W.V. Steele, R.D. Chirico, Thermodynamics and the hydrodeoxygenation of 2,3-benzofuran, U.S. Dep. Energy (1990).

[62] F.X. Cormerais, G. Perot, F. Chevalier, M. Guisnet, New evidence for ethers as intermediates in the conversion of dimetthyl ether into olefins, J. Chem. Res.-S (1980) 362-363.

[63] D. Li, P. Bui, H. Zhao, S.T. Oyama, T. Dou, Z.H. Shen, Rake mechanism for the deoxygenation of ethanol over a supported Ni_2P/SiO_2 catalyst, J. Catal. 290 (2012) 1-12.

[64] A. Cho, H. Kim, A. Iino, A. Takagaki, S. Ted Oyama, Kinetic and FTIR studies of 2-methyltetrahydrofuran hydrodeoxygenation on Ni_2P/SiO_2, J. Catal. 318 (2014) 151-161.

[65] P. Bui, S.T. Oyama, A. Takagaki, B. P. Carrow, K. Nozaki, Reactions of 2-methyltetrahydropyran on silica-supported nickel phosphide in comparison with 2-methyltetrahydrofuran, ACS Catal. 6 (2016) 4549-4558.

[66] F.E. Massoth, P. Politzer, M.C. Concha, J.S. Murray, J. Jakowski, J. Simons, Catalytic hydrodeoxygenation of methyl-substituted phenols: Correlations of kinetic parameters with molecular properties, J. Phys. Chem. B 110 (2006) 14283-14291.

[67] G.-N. Yun, S.J. Ahn, A. Takagaki, R. Kikuchi, S.T. Oyama, Infrared spectroscopic studies of the hydrodeoxygenation of γ-valerolactone on Ni_2P/MCM-41, Catal. Today, 323 (2019) 54-61.

[68] A. Iino, A. Cho, A. Takagaki, R. Kikuchi, S.T. Oyama, Kinetic studies of hydrodeoxygenation of 2-methyltetrahydrofuran on Ni_2P/SiO_2 catalyst at medium pressure, J. Catal. 311 (2014) 17.

[69] S. T. Oyama, Adsorbate bonding and the selection of partial and total oxidation pathways, J. Catal. 128 (1991) 210-217.

[70] M.A. Vannice, Kinetics of Catalytic Reactions, Springer, New York, 2005, Table 6.10, p.136

[71] M. Boudart, D. E. Mears, M.A. Vannice, Kinetics of heterogeneous catalytic reactions, Ind. Chem. Belg. 32 (1967) 281-284.

[72] S. T. Oyama, G.-N. Yun, S.-J. Ahn, K.K. Bando, A. Takagaki, R. Kikuchi, How to scrutinize adsorbed intermediates observed by in situ spectroscopy:Analysis of coverage transients (ACT), J. Catal. 394 (2021) 273-283.

[73] P. Agarwal, N. Evenepoel, S. S. Al-Khattaf, M. T. Klein, Molecular level kinetic modeling of methyl laurate: The intrinsic kinetics of triglyceride hydroprocessing, Energy Fuels 32 (2018) 5264-5270.

[74] I. Craciun, M. F. Reyniers, G. B. Marin, Effects of acid properties of Y zeolites on the liquid-phase alkylation of benzene with 1-octene: A reaction path analysis, J. Mol. Catal. A: Chem. 277 (2007) 1-14.

[75] V.-H. Nguyen, S.D. Lin, J.C.-S. Wu, Synergetic photo-epoxidation of propylene over VTi/MCM-41 mesoporous photocatalysts, J. Catal. 331 (2015) 217-227.

[76] J. Lauwaert, E. De Canck, D. Esquivel, J.W. Thybaut, P. Van Der Voort, G.B. Marin, Silanol-assisted aldol condensation on aminated silica: Understanding the arrangement of functional groups, ChemCatChem 6 (2014) 255-264.

[77] G.-N. Yun, I.T. Ghampson, W.J. Movick, V. Vargheese, Y. Kobayashi, S.T. Oyama, Applicability of the Delplot method for the determination of catalytic reaction sequences: Hydrodeoxygenation of γ-valerolactone on Ni_2P/MCM-41, Chem. Eng. Sci., 223 (2020) 115697.

Delplot Method Applied to Adsorbates